Accepted Manuscript

Design, synthesis, and biological evaluation of novel combretastatin A-4 thio derivatives as microtubule targeting agents

Tomasz Stefański, Renata Mikstacka, Rafał Kurczab, Zbigniew Dutkiewicz, Małgorzata Kucińska, Marek Murias, Małgorzata Zielińska-Przyjemska, Michał Cichocki, Anna Teubert, Mariusz Kaczmarek, Adam Hogendorf, Stanisław Sobiak

PII: S0223-5234(17)30953-4

DOI: 10.1016/j.ejmech.2017.11.050

Reference: EJMECH 9925

To appear in: *European Journal of Medicinal Chemistry*

Received Date: 27 September 2017

Revised Date: 17 November 2017

Accepted Date: 18 November 2017

Please cite this article as: T. Stefański, R. Mikstacka, Rafał. Kurczab, Z. Dutkiewicz, Mał. Kucińska, M. Murias, Mał. Zielińska-Przyjemska, Michał. Cichocki, A. Teubert, M. Kaczmarek, A. Hogendorf, Stanisł. Sobiak, Design, synthesis, and biological evaluation of novel combretastatin A-4 thio derivatives as microtubule targeting agents, *European Journal of Medicinal Chemistry* (2018), doi: 10.1016/j.ejmech.2017.11.050.

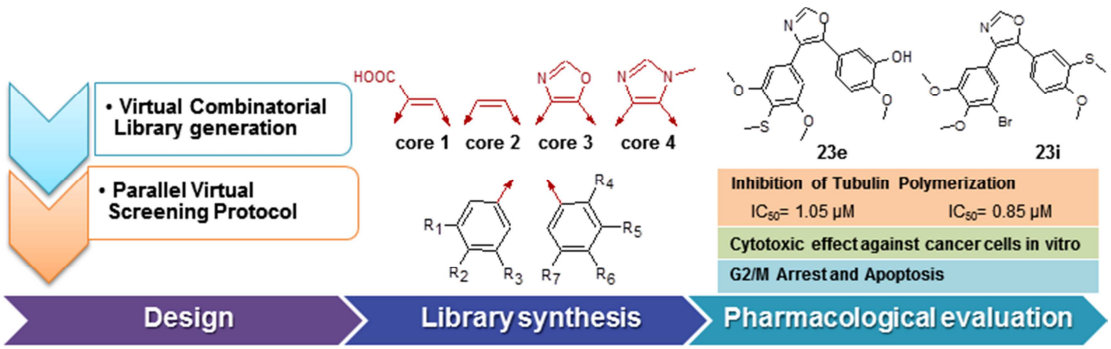

Design, synthesis, and biological evaluation of novel combretastatin A-4 thio derivatives as microtubule targeting agents

Tomasz Stefański,[1] Renata Mikstacka,[2] Rafał Kurczab,[3] Zbigniew Dutkiewicz,[1] Małgorzata Kucińska,[4] Marek Murias,[4] Małgorzata Zielińska-Przyjemska,[5] Michał Cichocki,[5] Anna Teubert,[6] Mariusz Kaczmarek,[7] Adam Hogendorf,[3] and Stanisław Sobiak[2]*

[1]Department of Chemical Technology of Drugs, Poznan University of Medical Sciences, Grunwaldzka 6, 60-780 Poznań, Poland

[2]Department of Inorganic and Analytical Chemistry, Collegium Medicum in Bydgoszcz, Nicolaus Copernicus University in Toruń, Jurasza 2, 85-089 Bydgoszcz, Poland

[3]Department of Medicinal Chemistry, Institute of Pharmacology, Polish Academy of Sciences, Smętna 12, 31-343 Kraków, Poland

[4]Department of Toxicology, Poznan University of Medical Sciences, Dojazd 30, 60-631 Poznań, Poland

[5]Department of Pharmaceutical Biochemistry, Poznan University of Medical Sciences, Święcickiego 4, 60-781 Poznań, Poland

[6]Institute of Bioorganic Chemistry, Polish Academy of Sciences, Noskowskiego 12/14, 61-704 Poznań, Poland

[7]Department of Immunology, Poznan University of Medical Sciences, Rokietnicka 5D, 60-806 Poznań, Poland

ABSTRACT: A series of novel combretastatin A-4 (CA-4) thio derivatives containing different molecular cores, namely α-phenylcinnamic acids (core 1), (*Z*)-stilbenes (core 2), 4,5-disubstituted oxazoles (core 3), and 4,5-disubstituted N-methylimidazoles (core 4), as *cis*-restricted analogues were designed and synthesized. They were selected with the use of a parallel virtual screening protocol including the generation of a virtual combinatorial library based on an elaborated synthesis protocol of CA-4 analogues. The selected compounds were evaluated for antiproliferative activity against a panel of six human cancer cell lines (A431, HeLa, MCF7, MDA-MB-231, A549 and SKOV) and two human non-cancer cell lines (HaCaT and CCD39Lu). Moreover, the effect of the test compounds on the inhibition of tubulin polymerization *in vitro* was estimated. In the series studied here, oxazole-bridged analogues exhibited the most potent antiproliferative activity. Compounds **23a**, **23e**, and **23i** efficiently inhibited tubulin polymerization with IC_{50} values of 0.86, 1.05, and 0.85 μM, respectively. Thio derivative **23i**, when compared to its oxygen analogue **23j**, showed a 5-fold higher inhibitory impact on tubulin polymerization. Compounds **23e** and **23i**, which showed both best cytotoxic and antitubulin activity, were further studied in terms of their effect on cell cycle distribution and proapoptotic activity. Compound **23e** induced a statistically significant block of the cell cycle at the G2/M phase in A431, HaCaT, HeLa, MCF-7, MDA-MB-231, and SKOV-3 cells to an extent comparable to that observed in CA-4. In HeLa and SKOV-3 cells incubated with **23i**, a concentration-dependent block of the G2/M phase was observed. The proapoptotic effect of **23e** and **23i** in A431, HaCaT, MCF-7, MDA-MB-231, and SKOV-3 was demonstrated with ELISA

assay and double staining with Annexin V-FITC/PI. The results indicated that compound **23e** and **23i** may serve as novel lead compounds in research on more effective anticancer agents.

Keywords: anticancer agents; tubulin polymerization inhibitors; combretastatin A-4; virtual screening; synthesis.

1. Introduction

Microtubules are highly dynamic components of the cytoskeleton that consist of *αβ*-tubulin heterodimers and are involved in a wide range of various cellular functions, including maintenance of the cell structure, motility, intercellular transport, and cell division, where they are responsible for mitotic spindle formation and proper chromosomal separation [1–4]. The biological importance of microtubules in mitosis and cell division as well as their dynamic nature makes them a significant and intensively investigated molecular target for anticancer drugs [5–11].

Microtubule-interfering agents (MIAs), of which several are natural products, act via two different mechanisms of action leading to either the inhibition or enhancement of tubulin polymerization. Both effects impair microtubule dynamics and have an impact on cell proliferation. MIAs bind to one of the three major different binding sites on tubulin, i.e. the taxol binding site, colchicine-binding site, and vinca alkaloid domain [5,6]. Ligands which stimulate microtubule polymerization, known as microtubule stabilizers such as paclitaxel or epothilone, bind to the taxol binding site [12,13]. In turn, microtubule destabilizers (tubulin polymerization inhibitors) induce depolymerization of microtubules. In this group, different vinca alkaloids can be distinguished, such as vinblastine and vincristine which bind to the vinca domain [14,15], and

a large class of ligands which interact with the colchicine-binding site, including colchicine (**2)**, podophyllotoxin (**3)**, steganacin (**4)**, and combretastatins [16–20].

Combretastatins are a group of natural *cis*-stilbenes that were isolated from the bark of the African bush willow tree *Combretum caffrum* over 30 years ago [21–24]. The most active member of this group as described by Pettit et al. [25] is combretastatin A-4 (CA-4, **1a**, Fig. 1), which presents remarkable biological activity that is manifested in strong inhibition of tubulin polymerization, potent *in vitro* cytotoxicity against a variety of human cancer cell lines, including multidrug resistant (MDR) cell lines overexpressing P-glycoprotein (Pgp), and *in vivo* efficacy as a vascular-disrupting agent (VDA) and antiangiogenic agent [25–29]. Its water-soluble prodrug, CA-4 disodium phosphate (CA-4P, **1b**, Fig. 1), has shown promising results in numerous clinical trials in both monotherapy and in combination with various anticancer agents, exhibiting high efficacy in the treatment of anaplastic thyroid cancer and ovarian cancer [30,31].

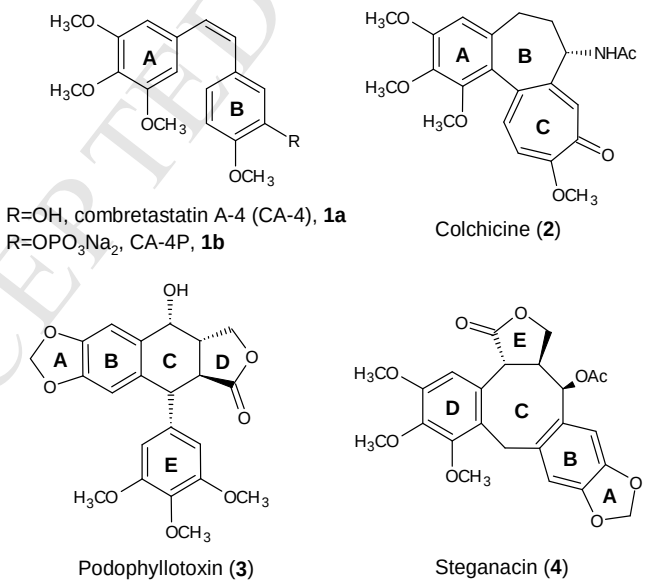

Fig. 1. Microtubule targeting agents with affinity for colchicine-binding site.

Promising results in anticancer therapy with CA-4's unique and multidirectional activity as well as its relatively simple structure as a lead make extensive structural modification that will improve its natural anticancer properties possible. Meanwhile, numerous structure-activity relationship (SAR) studies of CA-4 have been conducted leading to the identification of functional groups and their positions that are important to ensure optimal interactions with the colchicine binding site and efficacious antimitotic activity [29,32–37]. In general, these modifications pertained to the A-ring, B-ring, and/or ethylene bridge. They showed the importance of the 3,4,5-timethoxy substitution pattern on the A-ring, 4-methoxy substituted B-ring, and the *cis*-configured double bond, which are fundamental for the inhibitory activity of tubulin polymerization.

Bioisosterism is a widely used strategy for the rational design of new drugs including anticancer agents, particularly for designing agents with optimal pharmacological properties [38]. The compounds of the studied series of CA-4 derivatives possess an atom of bivalent oxygen replaced by sulfur. Our previous studies on methylthio-*trans*-stilbenes as chemopreventive agents showed the high affinity of selected thio derivatives to human recombinant CYPs, particulary CYP1A1 and CYP1B1 [39–42]. Other authors showed that the introduction of a less electronegative sulfur atom instead of the oxygen atom led to a reduction of toxicity in HEK 293 cells (human embryonic kidney cell line) and thus could improve selectivity for cancer cell lines [43]. Further modification of the CA-4 molecule, as taken into account in the design of our series, was an improvement of the stability of the designed CA-4 analogues because the ethylene bridge in CA-4 is able to undergo *cis*-*trans* isomerization, which causes complete loss of cytotoxicity. This was possible by replacing the olefinic double bond with five-member heterocyclic rings such as oxazole and N-methylimidazole. Several groups of

researchers have reported that this type of structural modification allows to avoid the stability problem and improves anticancer activity [44–54]. Such replacement allows to retain the correct geometric orientation of the phenyl rings of the CA-4 derivatives by placing them at an appropriate distance for optimal interaction with the colchicine-binding domain on tubulin.

In this paper we present the design, synthesis, and biological evaluation of a series of CA-4 thio derivatives with different molecular cores. The compounds were designed using a parallel virtual screening protocol including the generation of a virtual combinatorial library (VCL) based on an elaborated synthesis protocol of CA-4 analogues, 3-dimensional pharmacophore screening, two QSAR filters, docking to the colchicine binding site of tubulin, and a final ranking strategy. The selected derivatives were synthesized and evaluated for their effect on tubulin polymerization *in vitro*. Moreover, their antiproliferative activity was assessed in a panel of six human cancer (A431, HeLa, MCF7, MDA-MB-231, A549, SKOV3) and two non-cancer cell lines (HaCaT, CCD39Lu). The most potent compounds in the series **23e** and **23i** were further studied for cell cycle effects, apoptosis, and on a microtubule network.

2. Results and discussion

2.1. Virtual screening

A protocol including combinatorial library generation and screening was developed and tested to support the design of CA-4 thio analogues (Fig. 2). Based on an elaborated synthetic protocol for sulfur analogues of CA-4 (Scheme 2-6), different substituted aromatic aldehydes (BB1) and phenylacetic acids (BB2) were selected from an in-house library and used to generate the VCL by iterative combination of selected reagents. The obtained VCL (1,159 cmpds) was processed by the parallel virtual screening (VS) protocol including a 3-dimensional pharmacophore filter, two QSAR models, and the post-docking scoring method (for details, see

Supplementary Information). Based on the VS scores, 17 compounds (approx. 2% of VCL) that had different classification scores (from the worst to the best ones, i.e. 1-5) were selected and synthesized.

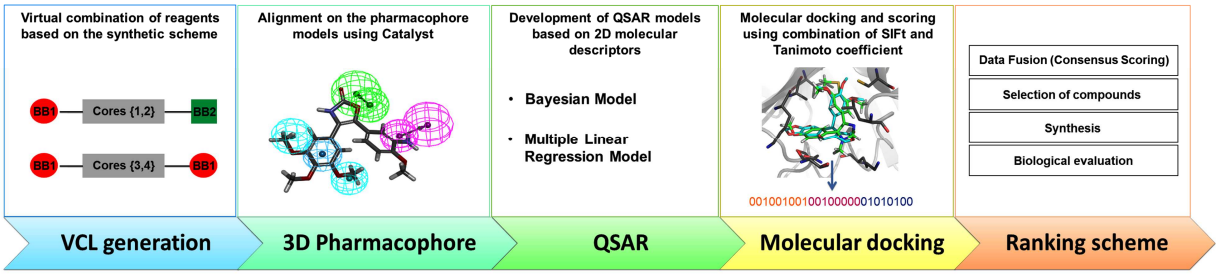

Fig. 2. Illustration of VCL-VS protocol applied for design CA-4 analogues.

To evaluate the real efficiency of the methodology used here, we assumed that the compound inhibited tubulin polymerization when its IC_{50} was lower than 10 μM. Based on this assumption and the predicted VS scores, the ROC curve with VS score cut-offs was plotted (Fig. 3). It showed very good predictive power of the applied VS protocol (AUROC and BEDROC were 0.85 and 1.00, respectively).

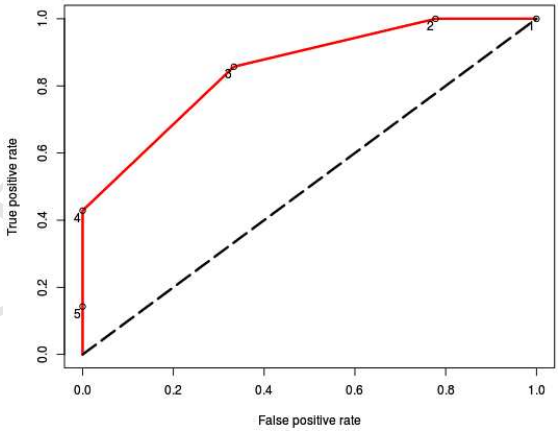

Fig. 3. The ROC curve showing real performance of virtual screening of VCL library.

Interestingly, when the VS score cut-off was greater or equal to 4 the sensitivity (true positive rate) was 0.43 and precision was 1.00. However, a VS score cut-off greater or equal to 3

is an optimal choice for virtual screening subjects because both sensitivity and precision are high (0.86 and 0.67, respectively).

2.2. Chemistry

CA-4 (**1a**) was prepared using the two-step procedure described by Gaukroger and co-workers [34] using Perkin-type condensation between 3,4,5-trimethoxyphenylacetic acid (**5)** and isovanillin (**6)** and subsequent decarboxylation of the obtained α-phenylcinnamic acid (**7)** (Scheme 1).

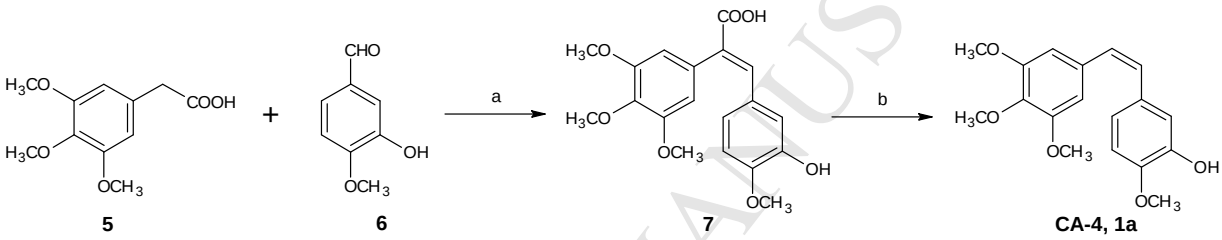

Scheme 1. Synthesis of CA-4. Reagents and conditions: (a) Ac_2O, Et_3N, 4 h, 110 ºC, 44%; (b) quinoline, Cu, 3 h, 200 ºC, 40%.

Preparation of the designed CA-4 derivatives differing in four molecular cores, namely α-phenylcinnamic acids (core 1, **14a-b**), (*Z*)-stilbenes (core 2, **15a-b**), 4,5-disubstituted oxazoles (core 3, **23a-j**), and 4,5-disubstituted N-methylimidazoles (core 4, **24a-f**), as *cis*-restricted analogues is illustrated in Schemes 2-6 following general procedures as detailed below and in the Experimental Section. Bromobenzaldehyde (**10**) [55] was prepared from commercially available vanillin (**8**) by its bromination and subsequent methylation of the obtained bromovanillin (**9**) [56] with methyl iodide. Methylthiobenzaldehydes **6d** [57], **8d** [58], **9d**, **11d** [57] and **12d** [59] were obtained in a multistep reaction starting from appropriately substituted hydroxybenzaldehydes **6**, **8-9** and **11-12** (Scheme 2). In the first step, the obtained O-aryl thiocarbamates **6a** [60], **8a** [58], **9a**, **11a** [61] and **12a** [59] were converted using a Newman-Kwart rearrangement to the

corresponding S-aryl thiocarbamates **6b**, **8b** [58], **9b**, **11b** [61] and **12b** [59] which were then readily hydrolyzed using methanolic potassium hydroxide to thiophenols, and in a one-pot reaction converted to final products by subsequent methylation with methyl iodide or dimethyl sulfate. In the preparation of benzaldehydes **9d** and **12d**, an additional step of protecting the carbonyl group in S-aryl thiocarbamates **9b** and **12b** was required by the formation of cyclic acetals, 1,3-dioxolanes **9c** and **12c**. Their hydrolysis, methylation, and deprotection were conducted in a one-pot reaction which allowed to obtain methylthiobenzaldehydes **9d** and **12d** in good yields.

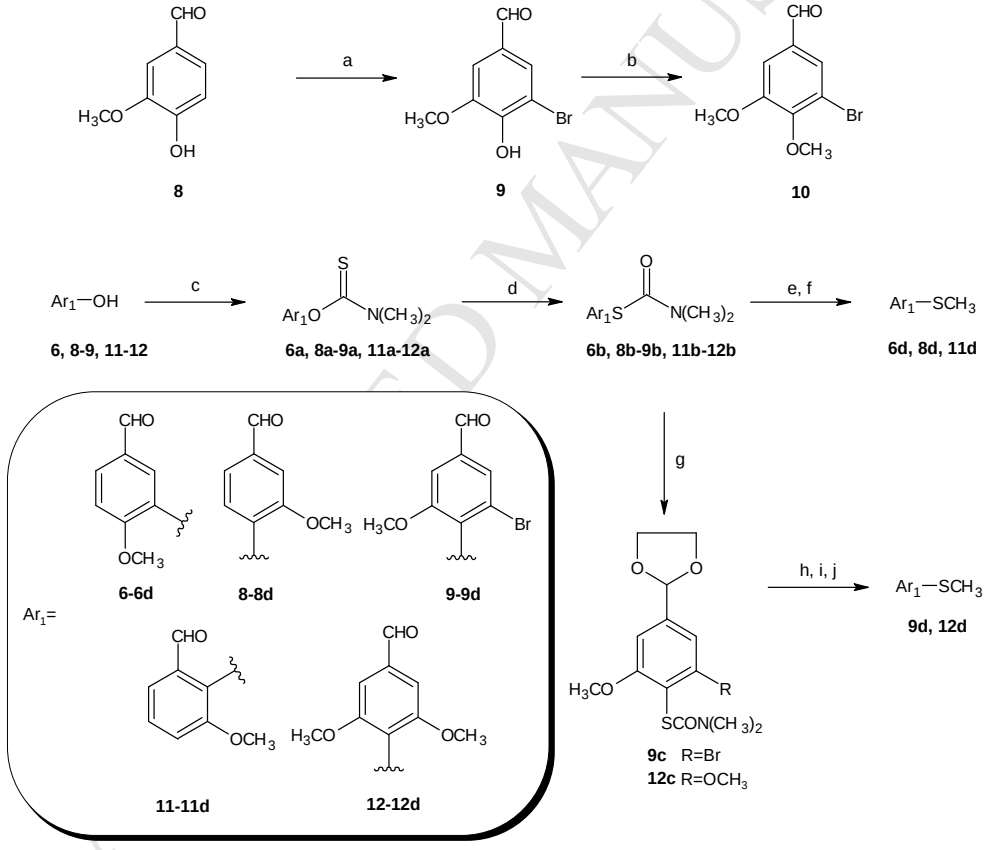

Scheme 2. Synthesis of bromo- (**9**, **10**) and methylthiobenzaldehydes (**6d**, **8d-9d**, **11d-12d**). Reagents and conditions: (a) Br_2, MeOH, 1 h, 0-25 ºC, 99%; (b) methyl iodide, K_2CO_3, DMF, 24 h, rt, 88%; (c) H_2O, KOH, N,N-dimethylthiocarbamoyl chloride, THF, 1-1.5 h, 0-25 ºC, 63-94%; (d) diphenyl ether, 15-120 min, 240 ºC, 54-94%; (e) KOH (10% in MeOH), 2-7 h, 80 ºC; (f) methyl iodide, 24 h, 25 ºC, 67-98% (e and f); (g) ethylene glycol, *p*-toluenesulfonic acid monohydrate, toluene, 2.5 h, 145 ºC, 77-94%; (h) KOH

(10% in MeOH), 3-7 h, 80 ºC; (i) Me_2SO_4, 1 h, 25-55ºC; (j) 5% HCl (pH=2-3), 2h, 55ºC, 67-98% (h, i and j).

The synthesis of α-phenylcinnamic acids **14a-b** [62,63] possessing core 1 and (*Z*)-stilbenes **15a-b** [62,63] with core 2 (Scheme 3) was conducted in a manner similar to the preparation of CA-4. The geometries of the (*Z*)-stilbenes were confirmed by their characteristic ^{1}H NMR coupling constants for olefinic protons of ca. 12–12.1 Hz.

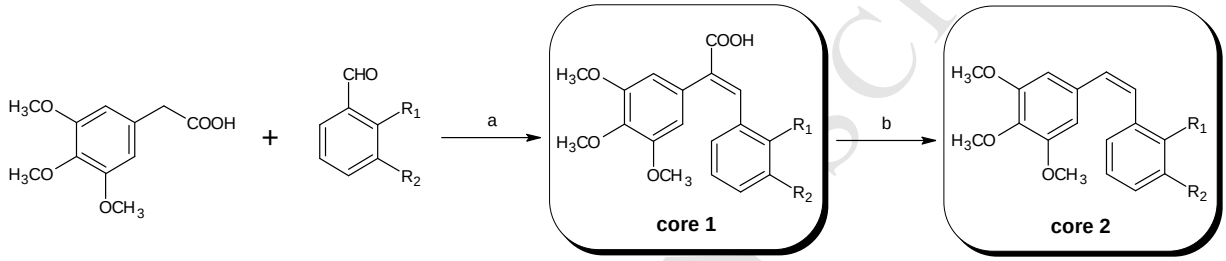

5

11d R_1=SCH_3, R_2=OCH_3
13 R_1=SCH_3, R_2=H

14a R_1=SCH_3, R_2=OCH_3
14b R_1=SCH_3, R_2=H

15a R_1=SCH_3, R_2=OCH_3
15b R_1=SCH_3, R_2=H

Scheme 3. Synthesis of *α*-phenylcinnamic acids (**14a-b**) and (*Z*)-stilbenes (**15a-b**). Reagents and conditions: (a) Ac_2O, Et_3N, 4 h, 115 ºC, 34-40%; (b) quinoline, Cu, 2.5 h, 200 ºC, 37-39%.

The new oxazole-bridged CA-4 analogues **23a-j** [62,63] (core 3) (Scheme 5) and N-methylimidazole-bridged analogues **24a-f** [62,63] (core 4) (Scheme 6) were prepared using the Van Leusen multicomponent reaction between corresponding benzaldehydes and *p*-toluenesulfonylmethyl isocyanides (TosMICs) **20-22** [44,64] whose synthesis is shown in Scheme 4.

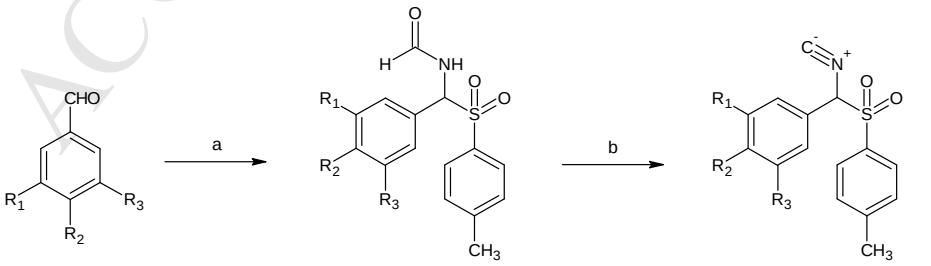

10 R_1=R_2=OCH_3, R_3=Br
12d R_1=R_3=OCH_3, R_2=SCH_3
16 R_1=R_2=R_3=OCH_3

17 R_1=R_2=OCH_3, R_3=Br
18 R_1=R_3=OCH_3, R_2=SCH_3
19 R_1=R_2=R_3=OCH_3

20 R_1=R_2=OCH_3, R_3=Br
21 R_1=R_3=OCH_3, R_2=SCH_3
22 R_1=R_2=R_3=OCH_3

Scheme 4. Synthesis of TosMIC derivatives (**20-22**). Reagents and conditions: (a) $HCONH_2$, *p*-toluenesulfinic acid, CSA, 20 h, 60 ºC, 57-72%; (b) $POCl_3$, Et_3N, DME, 2-3 h, -5 ºC, 70-75%

The appropriate substituted benzaldehydes obtained earlier, **10** and **12d,** or commercially available **16**, were reacted with freshly prepared *p*-toluenesulfinic acid and formamide, catalyzed by 10-camphorsulfonic acid (CSA) to give tosylmethyl formamides **17-19** [44,64]. Dehydration with $POCl_3$ afforded the desired TosMICs **20-22**. Preparation of N-methylimidazole-bridged analogues (Scheme 6) involved the first generation of aldimines resulting from the reaction of appropriate benzaldehydes and methylamine and then their condensation with TosMICs in the presence of anhydrous K_2CO_3.

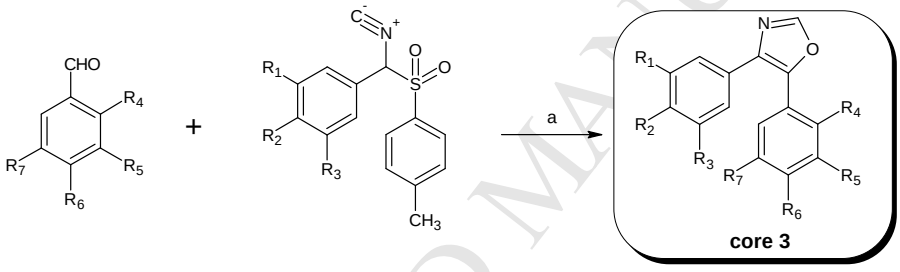

6a-d, 8d, 9d, 13 **20-22**

23a $R_1=R_2=R_3=OCH_3$, $R_4=SCH_3$, $R_{5\text{-}7}=H$

b → **23b** $R_1=R_2=R_3=R_6=OCH_3$, $R_{4,7}=H$, $R_5=SC(O)N(CH_3)_2$

b → **23c** $R_1=R_2=R_3=R_6=OCH_3$, $R_{4,7}=H$, $R_5=SH$

b → **23d** $R_1=R_3=R_6=OCH_3$, $R_2=SCH_3$, $R_{4,7}=H$, $R_5=OC(S)N(CH_3)_2$

23e $R_1=R_3=R_6=OCH_3$, $R_2=SCH_3$, $R_{4,7}=H$, $R_5=OH$

23f $R_1=R_2=R_3=R_5=OCH_3$, $R_{4,7}=H$, $R_6=SCH_3$

23g $R_1=R_2=R_3=R_7=OCH_3$, $R_4=H$, $R_5=Br$, $R_6=SCH_3$

23h $R_1=R_2=R_5=OCH_3$, $R_3=Br$, $R_{4,7}=H$, $R_6=SCH_3$

23i $R_1=R_2=R_6=OCH_3$, $R_3=Br$, $R_{4,7}=H$, $R_5=SCH_3$

23j $R_1=R_2=R_5=R_6=OCH_3$, $R_3=Br$, $R_{4,7}=H$

Scheme 5. Synthesis of oxazole-bridged analogues (**23a-j**). Reagents and conditions: (a) K_2CO_3, DME/MeOH, 2h, reflux, 36-62%; (b) KOH (10% in MeOH), 2 h, 80 ºC, 55-62%.

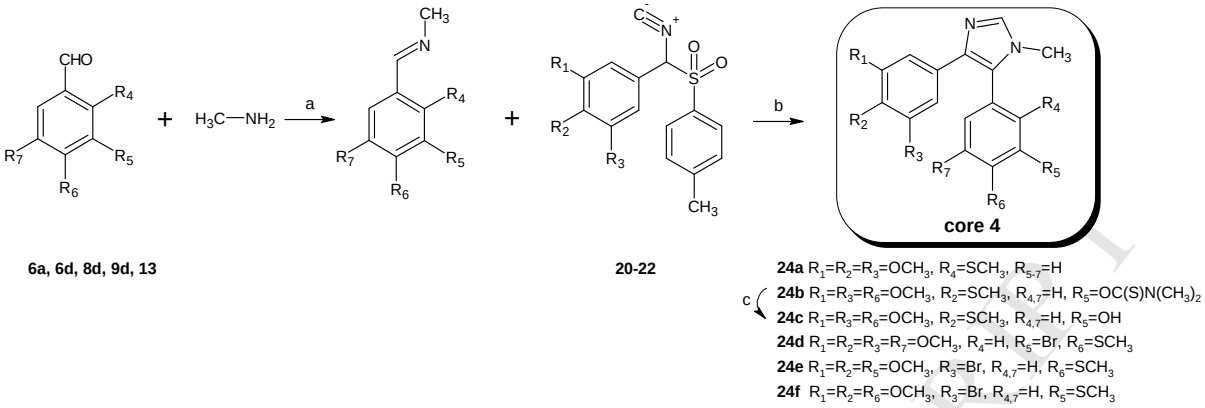

Scheme 6. Synthesis of N-methylimidazole-bridged analogues (**24a-f**). Reagents and conditions: (a) AcOH, EtOH, 2h, reflux; (b) K_2CO_3, DME, 3h, reflux, 27-92% (a and b); (c) KOH (10% in MeOH), 5.5 h, 80 ºC, 33%.

Preparation of heterocycle-based derivatives **23c, 23e,** and **24c** possessing the mercapto or hydroxy group involved synthesis of their S-aryl thiocarbamate or O-aryl thiocarbamate analogues followed by basic hydrolysis of the carbamate groups.

2.3. Biological evaluation

2.3.1. In vitro cytotoxic activities

Table 1 summarizes the cytotoxic effects of the obtained CA-4 analogues with each molecular core, namely α-phenylcinnamic acids (**14a-b**), (*Z*)-stilbenes (**15a-b**), 4,5-disubstituted oxazoles (**23a**, **23c**, **23e-j**), and 4,5-disubstituted N-methylimidazoles (**24a**, **24c-f**), against a panel of six human cancer cell lines (A431, HeLa, MCF7, MDA-MB-231, A549, and SKOV) and two human non-cancer cell lines (HaCaT and CCD39Lu), using CA-4 as the reference compound.

Table 1. Cytotoxic activities of **14a-b**, **15a-b**, **23a**, **23c**, **23e-j**, **24a**, **24c-f** and CA-4 against human cancer and non-cancer cell lines

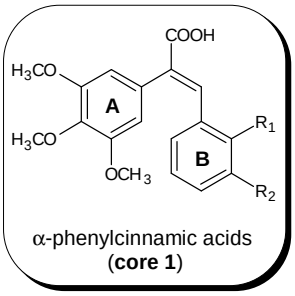

α-phenylcinnamic acids
(**core 1**)

14a R_1=SCH_3, R_2=OCH_3
14b R_1=SCH_3, R_2=H

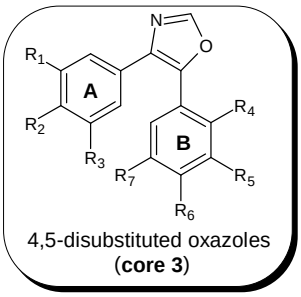

4,5-disubstituted oxazoles
(**core 3**)

23a R_1=R_2=R_3=OCH_3, R_4=SCH_3, $R_{5\text{-}7}$=H
23c R_1=R_2=R_3=R_6=OCH_3, $R_{4,7}$=H, R_5=SH
23e R_1=R_3=R_6=OCH_3, R_2=SCH_3, $R_{4,7}$=H, R_5=OH
23f R_1=R_2=R_3=R_5=OCH_3, $R_{4,7}$=H, R_6=SCH_3
23g R_1=R_2=R_3=R_7=OCH_3, R_4=H, R_5=Br, R_6=SCH_3
23h R_1=R_2=R_5=OCH_3, R_3=Br, $R_{4,7}$=H, R_6=SCH_3
23i R_1=R_2=R_6=OCH_3, R_3=Br, $R_{4,7}$=H, R_5=SCH_3
23j R_1=R_2=R_5=R_6=OCH_3, R_3=Br, $R_{4,7}$=H

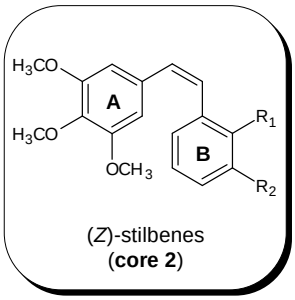

(*Z*)-stilbenes
(**core 2**)

15a R_1=SCH_3, R_2=OCH_3
15b R_1=SCH_3, R_2=H

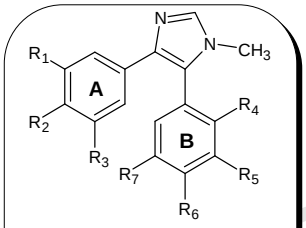

4,5-disubstituted N-methyl-imidazoles
(**core 4**)

24a R_1=R_2=R_3=OCH_3, R_4=SCH_3, $R_{5\text{-}7}$=H
24c R_1=R_3=R_6=OCH_3, R_2=SCH_3, $R_{4,7}$=H, R_5=OH
24d R_1=R_2=R_3=R_7=OCH_3, R_4=H, R_5=Br, R_6=SCH_3
24e R_1=R_2=R_5=OCH_3, R_3=Br, $R_{4,7}$=H, R_6=SCH_3
24f R_1=R_2=R_6=OCH_3, R_3=Br, $R_{4,7}$=H, R_5=SCH_3

Compd	IC_{50} (μM)[a]							
	A431	HeLa	MCF7	MDA-MB-231	A549	SKOV3	HaCaT	CCD39Lu
14a	>20	>20	0.95±0.33	>20	>20	>20	>20	>20
14b	>20	>20	1.84±0.36	>20	>20	>20	>20	>20
15a	3.61±2.44	6.18±0.46	0.65±0.19	11.73±0.85	>20	14.47±1.25	9.56±3.03	>20
15b	8.22±2.66	11.68±2.54	2.35±1.04	14.20±0.54	>20	14.08±0.61	12.82±1.83	>20
23a	>20	7.33±0.91	1.43±0.37	>20	>20	>20	>20	>20
23c	1.22±0.82	4.44±0.97	2.11±0.57	2.87±0.34	>20	3.18±0.26	1.28±0.15	>20
23e	0.25±0.20	0.009±0.002	0.45±0.14	0.71±0.16	>20	0.25±0.12	0.32±0.09	>20
23f	0.43±0.29	0.645±0.03	0.60±0.10	0.85±0.13	>20	1.48±0.16	0.43±0.13	>20
23g	>20	>20	1.42±0.23	17.87±0.90	>20	>20	16.74±2.64	>20
23h	0.41±0.10	0.44±0.04	2.48±0.64	0.76±0.10	>20	1.03±0.12	0.26±0.10	>20
23i	0.43±0.11	0.63±0.04	2.78±0.77	0.92±0.14	>20	1.16±0.13	0.52±0.08	>20
23j	12.32±0.25	0.07±0.04	6.10±1.05	7.83±1.18	0.50±0.18	0.26±0.18	10.09±1.96	>20
24a	>20	>20	2.29±0.46	>20	>20	>20	>20	>20
24c	0.43±0.13	0.39±0.02	1.63±0.27	0.39±0.28	>20	1.72±0.14	0.50±0.09	>20
24d	16.57±3.71	8.18±2.28	2.51±0.87	>20	>20	>20	>20	6.13±0.75

24e	13.64±3.23	>20	2.20±0.57	15.45±0.37	>20	>20	>20	19.26±2.14
24f	>20	>20	5.24±1.11	>20	>20	>20	>20	>20
CA-4	0.25±0.08	0.11±0.06	0.17±0.04	0.56±0.08	>20	0.38±0.09	0.19±0.08	0.009±0.002

[a] IC_{50} – compound concentration required to inhibit cell proliferation by 50%. Data are expressed as the mean ± SD from dose-response curves of three independent experiments.

The results listed in Table 1 indicate that cytotoxicity toward cancer cells varied between each molecular core. Compounds **14a-b** as analogues possessing the α-phenylcinnamic acid core (core 1) were generally inactive against the cancer cell lines (IC_{50} > 20μM), except for MCF7 from estrogen-dependent breast cancer adenocarcinoma, toward which they displayed relatively high antiproliferative activity (IC_{50} values of 0.95-1.84 μM).

In turn, compounds **15a-b** containing the (*Z*)-stilbene scaffold (core 2) with the same substituents in the phenyl rings displayed slightly enhanced activity toward four cancer cell lines (A431, HeLa, MDA-MB-231, and SKOV3) with IC_{50} values of 3.61-14.47 μM, while activity against MCF7 cells was retained.

The oxazole-bridged CA-4 analogues (core 3) generally displayed the best antiproliferative activity from all of the tested compounds toward the cancer cell lines except for A549, toward which most of the compounds were inactive. The number and position of the substituents in the phenyl B-ring had a major influence on antiproliferative activity. Compounds with substituents at 3,4-position of the phenyl B-ring showed much higher activity than compound **23a** with the -SCH_3 group at the *orto*-position or compound **23g** with substituents at 3,4,5-position in the phenyl B-ring. Replacement of the *m*-OCH_3 group in the trimethoxyphenyl A-ring (compound **23f**) with an electron withdrawing bromine atom (compound **23h**) maintained antiproliferative activity.

The most active compound, **23e**, in this series and of all the tested compounds was over 10-fold more potent against HeLa cells than the reference compound CA-4 with an IC_{50} value of 0.009 μM vs 0.11 μM, respectively. Interestingly, bioisosteric replacement of the oxygen atom with a sulfur atom (introduction of the *m*–SCH_3 group in compound **23i** instead of the *m*–OCH_3 group in compound **23j**) led to an increase in antiproliferative activity toward the A431 (28.7-fold), MCF7 (2.2-fold), and MDA-MB-231 (8.5-fold) cell lines. On the other hand, only compound **23j** was active against the highly drug-resistant A549 lung adenocarcinoma with an IC_{50} value of 0.5 μM.

N-methylimidazole-bridged CA-4 analogues (**24a**, **24e,** and **24f**) (core 4) were significantly less active than their corresponding oxazole analogues (**23a**, **23h**, and **23i**) when compared to the results of **23a** vs **24a**, **23h** vs **24e**, and **23i** vs **24f**, thus suggesting that replacement of the oxazole with the N-methylimidazole moiety was the major reason for the loss of activity in these compounds. Compound **24c** as an imidazole-bridged analogue of **23e** was only active in this series.

Because the toxicity of antitumor drugs toward normal tissues is a very important issue in chemotherapy, we evaluated the cytotoxic effects of these derivatives on normal human cells. For this purpose, all compounds were tested *in vitro* in human immortalized keratinocytes HaCaT and lung fibroblasts CCD39Lu. Based on the results, most of the compounds, with the exception of **24d**, showed slight cytotoxicity on fibroblast cells (IC_{50} > 20 μM) in contrast to the reference compound CA-4 (IC_{50} of 0.009 μM). However, some of the tested derivatives (**23c**, **23e**, **23f**, **23h**, **23i** and **24c**) were cytotoxic against immortalized human keratinocytes HaCaT (IC_{50} values of 0.32-1.28 μM verus 0.19 μM for CA-4).

Finally, two of the most active compounds (**23e** and **23i**) and six of the most sensitive cell lines (A431, HaCaT, HeLa, MCF-7, MDA-MB-231, and SKOV-3) were selected for further studies such as assessment of the cell cycle, tubulin staining (effect on microtubule dynamics), and apoptosis induction.

2.3.2. Inhibition of tubulin polymerization

Compounds **14a-b**, **15a-b**, **23a**, **23c**, **23e-j**, **24a**, and **24c-f** were investigated for their effect on tubulin polymerization with the use of turbidimetric assay *in vitro*. The N-methylimidazole-bridged analogues, unlike oxazole-bridged analogues, were poor tubulin polymerization inhibitors (Table 2). In the series of oxazole-bridged analogues, compounds **23a**, **23e**, and **23i** efficiently inhibited tubulin polymerization with an IC_{50} of 0.86, 1.05, and 0.85 μM, respectively (Table 2). CA-4 was used as a reference compound.

Table 2. Inhibition of tubulin polymerization and VS score for compounds **14a-b**, **15a-b**, **23a**, **23c**, **23e-j**, **24a**, **24c-f** and CA-4

Compd	IC_{50} (μM)[a]	VS score[b]
14a	>10	1
14b	>10	2
15a	>10	3
15b	>10	2
23a	0.86 (0.54-1.37)	3
23c	2.97 (2.36-3.73).	4
23e	1.05 (0.65-1.69)	5
23f	1.62 (0.94-2.80)	3

23g	>10	2
23h	1.54 (1.33-1.79)	3
23i	0.85 (0.54-1.31)	2
23j	4.80 (3.69-7.26)	3
24a	>10	3
24c	6.67 (6.37-6.98)	4
24d	>10	1
24e	>10	2
24f	>10	3
CA-4	2.72 (2.20-3.37)	5

[a] Tubulin polymerization was monitored spectrophotometrically at 340 nm for 1 h at 37˚C. The experiments were performed twice in duplicate. In parentheses 95% confidence intervals determined with the use of GraphPad Prism 5 are presented.

[b] Virtual Screening (VS) score was obtained according to the ranking scheme described in Experimental Section.

Compound **23j** as an oxygen analogue of **23i** weakly inhibited tubulin polymerization with IC_{50} equal to 4.80 μM. It should be noted that this outcome is in line with predictions obtained in the post-docking scoring strategy combining Tanimoto and SIFt (for details, see Supplementary Information), where the sulfur analogue was scored higher than the oxygen analogue.

2.3.3. Analysis of cell cycle and tubulin staining

In this experiment, the effect of the tested compounds on the cell cycle was assayed in six selected cancer cell lines; camptothecin at a concentration of 50 nM was used as a positive control (Fig. 4).

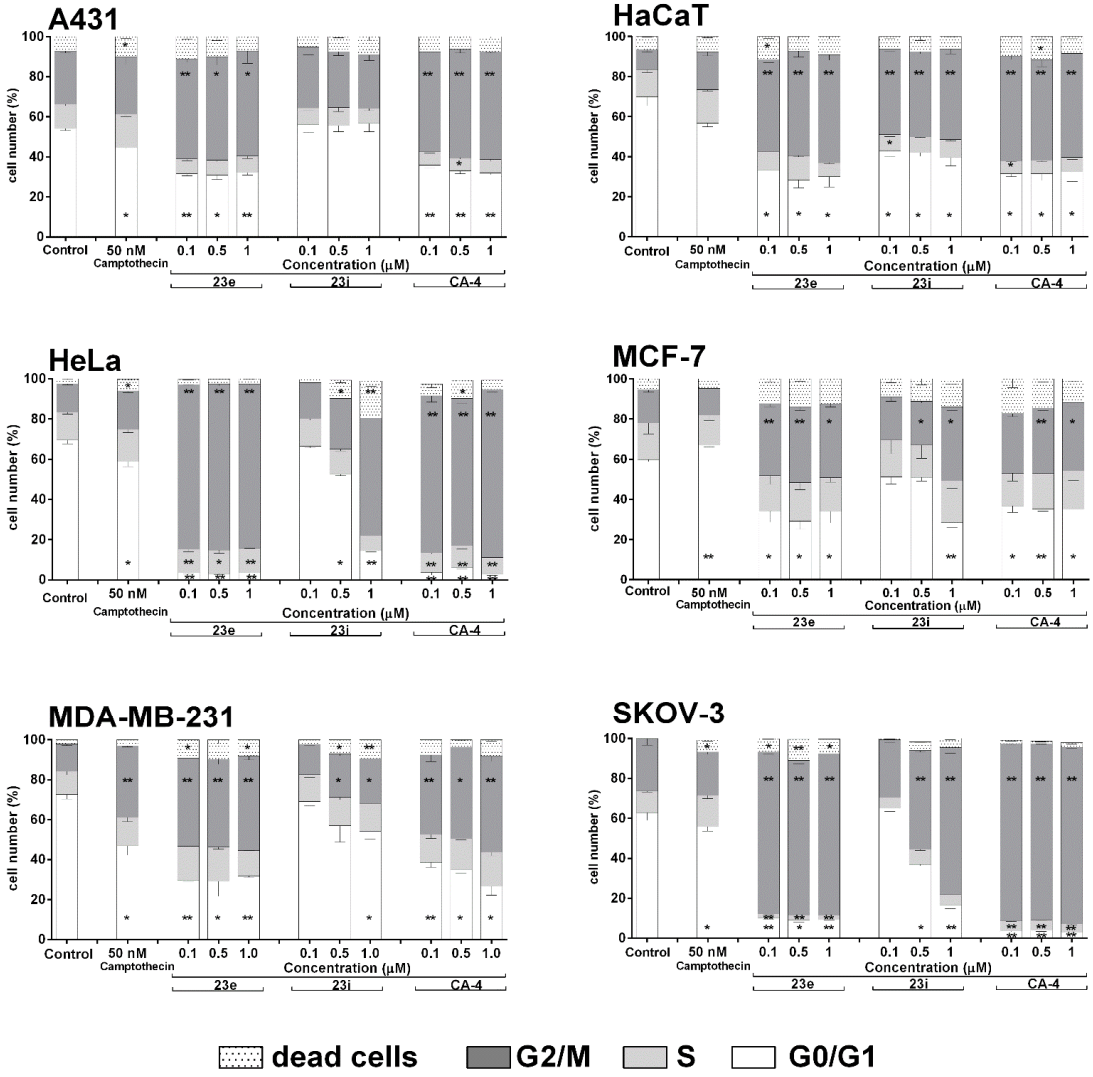

Fig. 4. Effect of **23e**, **23i** and CA-4 on cell cycle distribution in A431, HaCaT, HeLa, MCF-7, MDA-MB-231 and SKOV-3 cells. Cell cycle was monitored by flow cytometric analysis at 24 h after cells were treated with tested compounds. Data are expressed as mean ± SD of three independent experiments: (*) $p < 0.05$, (**) $p < 0.01$. Statistical significance between groups was assessed by Dunnett's Multiple Comparison Test.

Although all three of the tested compounds were shown to be able to inhibit polymerization of tubulin (Table 2), their impact on the cell cycle was significantly cell line-dependent.

Interestingly, very similar changes in cell cycle distribution were observed in the HeLa and SKOV-3 cell lines. Compound **23e** induced a statistically significant concentration-independent block of SKOV-3 cells in G2/M, while a similarly massive G2/M block was observed after incubation with CA-4. In contrast, after incubation with compound **23i** in HeLa and SKOV-3 cells, the concentration-dependent block of the G2/M phase was shown.

A similar trend was observed in A431, HaCaT, MCF-7, and MA-MB-231 cells treated with compounds **23e**, **23i**, and CA-4. The tested compounds were also investigated for their inhibition of tubulin polymerization using immunostaining (Fig. 5).

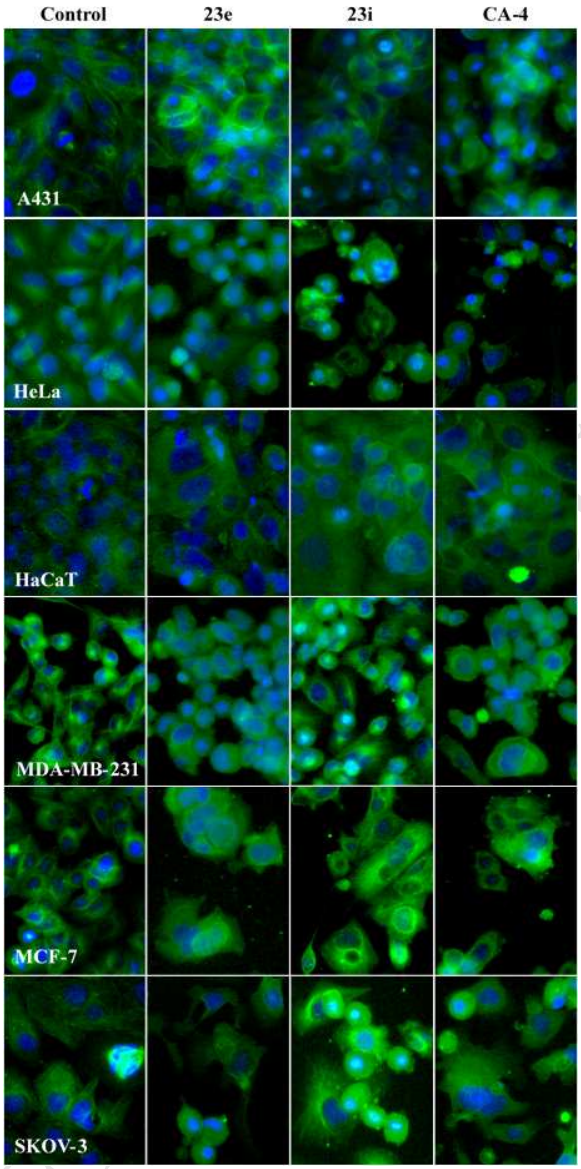

Fig. 5. Effect of **23e**, **23i** and CA-4 on tubulin polymerization and microtubules and nuclear condensation in A431, HeLa, HaCaT, MDA-MB-231, MCF-7 and SKOV-3 cells. Cells were treated with **23e**, **23i** and CA-4 at concentration of 1 μM for 24h. The control (intact) cells are presented in the first column on the left. The morphology of microtubules was visualized by staining with anti-alpha-tubulin antibodies connected with FITC (green), while the morphology of nuclei condensation was shown by staining with Hoechst 33258 (blue).

It is worth noting that besides disturbances in tubulin polymerization as shown in all of the tested cells, condensation of chromatin (stained with Hoechst 33358 dye) which is also typical for apoptosis, could be observed in the nuclei of cells incubated with **23i** (Fig. 5). Perturbations in the cytoskeleton structure as well as micronuclei formation corresponded with the results of ELISA and flow cytometry studies, where clear differences between effects exerted on cells by **23e**, CA-4, and, to a lesser extent, by **23i** could also be observed.

2.3.4. Induction of apoptosis

Induction of apoptosis in cells incubated with compounds **23e**, **23i**, and CA-4 was analyzed using two different methods. The ELISA assay measures the presence of markers for apoptotic cells, which was based on the quantitative detection of histone-associated DNA fragments in mono- and oligonucleosomes, while staining with Annexin V allows to detect phosphatidylserine externalization. Translocation of phosphatidylserine from the inner to the outer leaflet of the membrane is observed in intermediate stages of apoptosis and may be shown using Annexin V-FITC staining followed by flow cytometry. For cells incubated with **23e, 23i**, and CA-4, a clear concentration-dependent statistically significant increase of Annexin V positive cells was observed (Fig. 6).

Interestingly, in cells incubated with **23e**, the highest level of histone-associated DNA fragments in mono- and oligonucleosomes was observed only at the lowest concentration of **23e** and CA-4**,** while changes observed in cells incubated with **23i** may be described as concentration-dependent (Fig. 7).

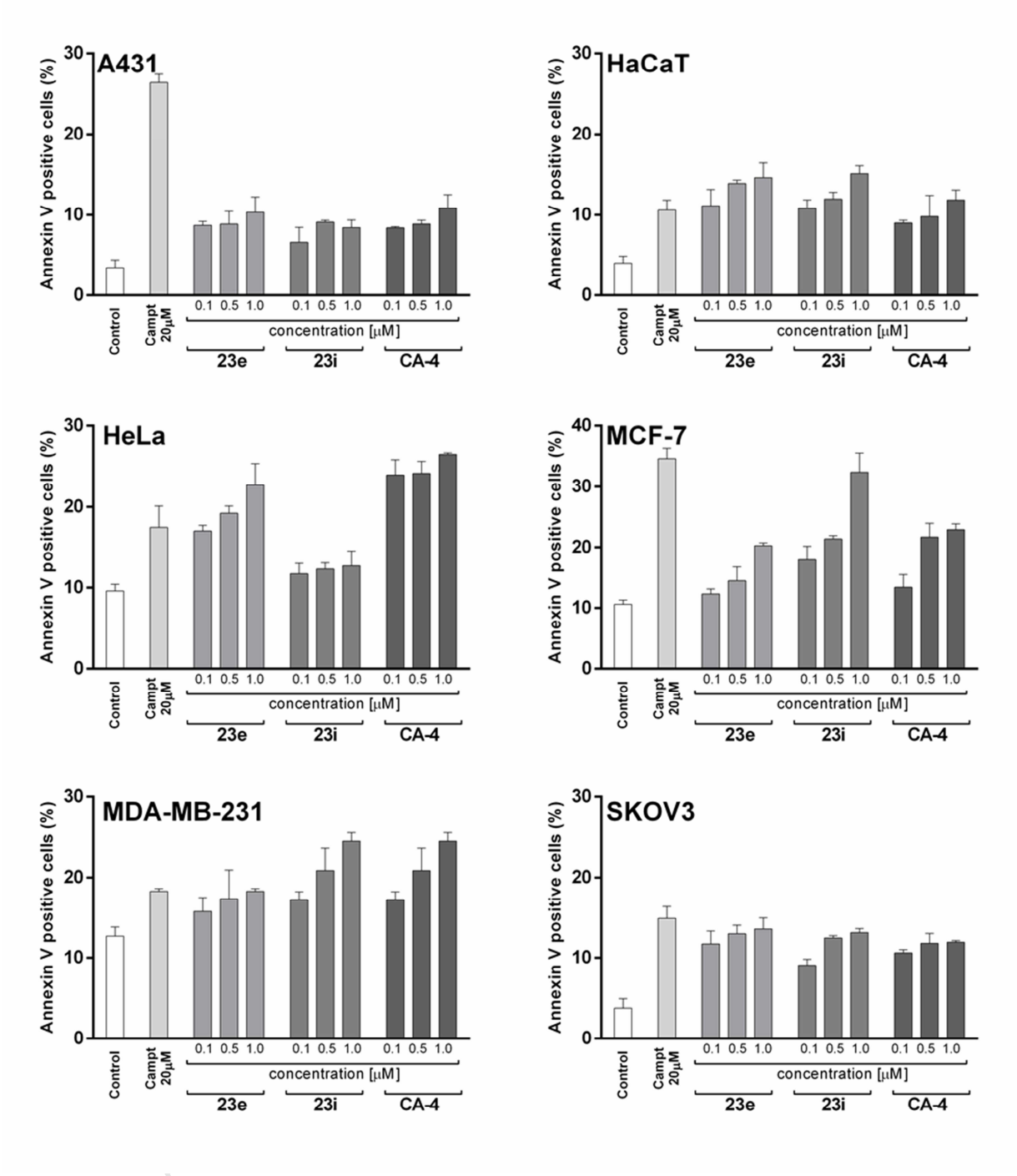

Fig. 6. CA-4 thio derivatives **23e** and **23i** increase apoptosis in A431, HaCaT, HeLa, MCF-7, MDA-MB-231 and SKOV-3 cells. Apoptosis was detected after 24 h of incubation with tested compounds by Annexin V-FITC/PI double staining by flow cytometry. Data are expressed as mean ± SD of three

independent experiments. Statistical significance between groups was assessed by Dunnett's Multiple Comparison Test. All treated groups were significantly different from control at $p < 0.05$.

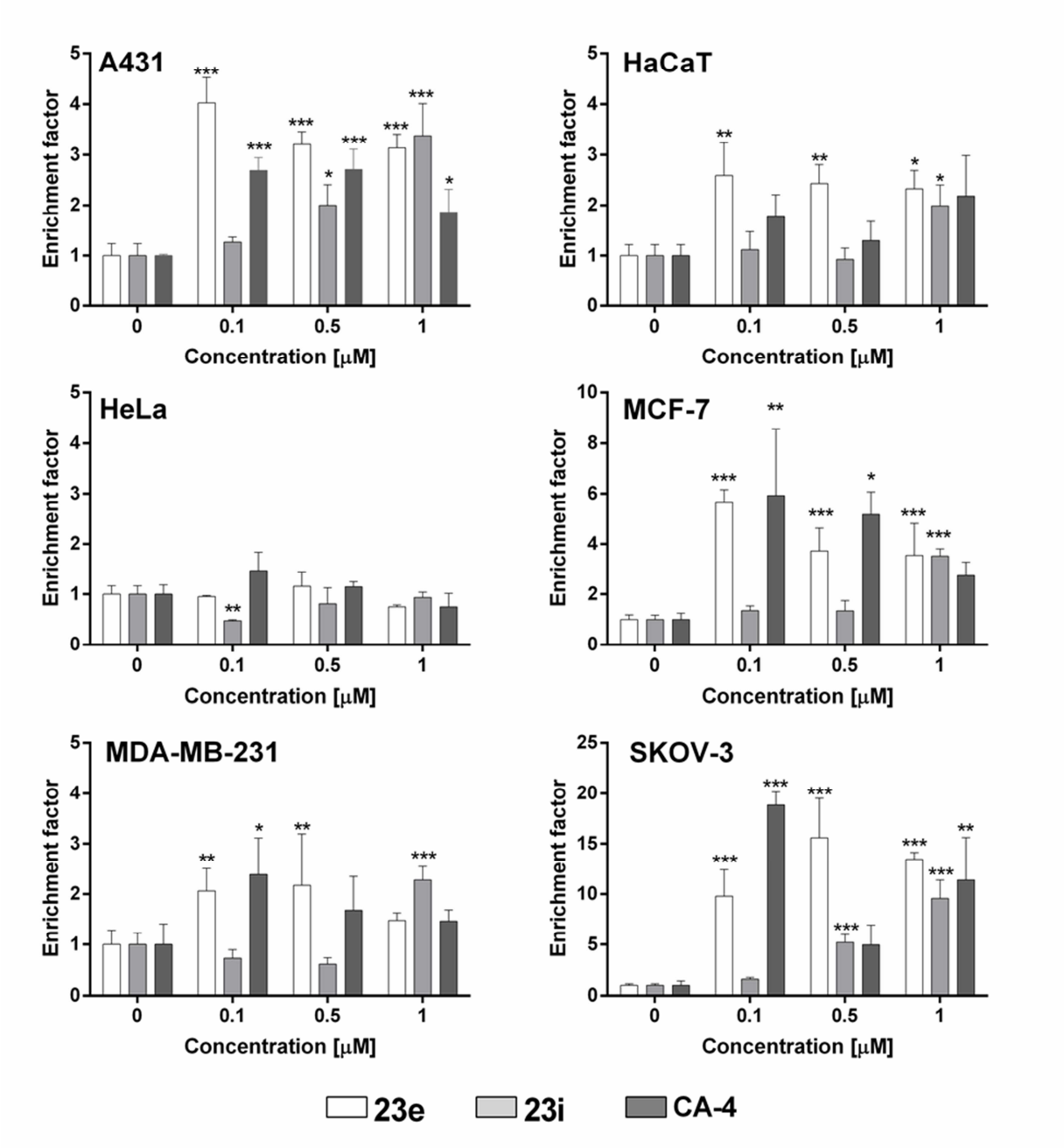

Fig. 7. Apoptosis detection using Cell Death Detection ELISA^{PLUS} followed by 24 h incubation of A431, HaCaT, HeLa, MCF-7, MDA-MB-231 and SKOV-3 cells with **23e**, **23i** and CA-4. Data are expressed as

mean ± SD of three independent experiments. Statistical significance is indicated with asterisks: ***p < 0.001, **p < 0.01 and *p < 0.05 indicate a significant difference from the control.

These results may suggest significant differences in the cellular uptake, metabolism, and cellular efflux of these cells as well as coexistence of different cellular signaling pathways stimulated by these compounds, although subsequent tests are necessary in order to fully explain these mechanisms.

2.3.5. Molecular modeling

Docking studies revealed that the binding modes of the most active compounds (**23e** and **23i)** are coherent with co-crystallized DAMA-colchicine (Fig. 8). The trisubstituted phenyl A-ring of **23e** and **23i** is buried in the *β*-subunit occupying the same position as the corresponding ring of colchicine.

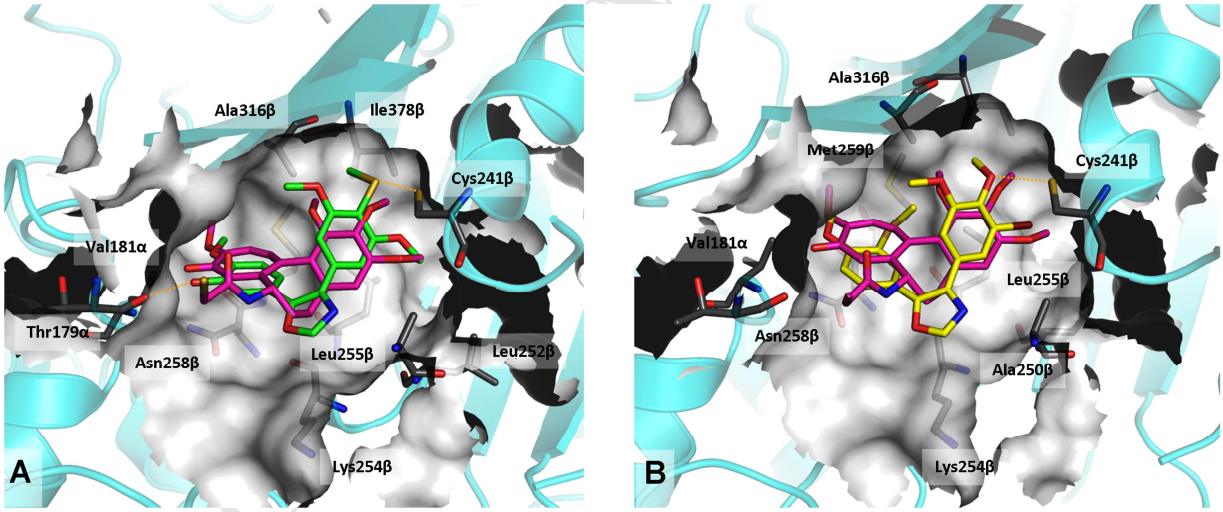

Fig. 8. The binding mode of A) **23e** (green) and B) **23i** (yellow) with DAMA-colchicine (magenta) in the *β*-tubulin binding site (PDB code 1SA0). Hydrogen bonding was depicted as orange dotted lines.

The thiol group of Cys241*β* forms a hydrogen bond with the sulfur or oxygen atom of the methylthio or methoxy group in *para*-position in **23e** and **23i**, respectively. In the most active

compound **23e,** the -SCH_3 group (ring A) is involved in hydrophobic interaction with the side chain of Leu255*β*, Ala316*β*, and Ile378*β*. The bromine atom in **23i** is placed in a position that allows hydrophobic interactions with Cys241*β*, Ala250*β*, and Leu255*β*. Moreover, the -SCH_3 substituent (**23i**, ring B) remains in close contact with Ala316*β*, Leu255*β*, and Met259*β*, thus making non-bonded S···S interaction with the sulfur atom of Met259*β* possible. It should be noted that oxazole derivatives (**23e** and **23i**) showed a similar binding mode with other *cis*-restricted analogues of CA-4 containing five-member aromatic heterocyclic rings, such as thiazoles [47], triazoles [46], and terazoles [48] with the trimethoxyphenyl ring placed in proximity of Cys241*β*.

3. Conlusions

We designed and synthesized a series of CA-4 thio derivatives containing different molecular cores, namely α-phenylcinnamic acids (core 1), (*Z*)-stilbenes (core 2), 4,5-disubstituted oxazoles (core 3), and 4,5-disubstituted N-methylimidazoles (core 4) as *cis*-restricted analogues. Compounds for synthesis were selected with the use of a parallel virtual screening protocol which showed a good predictive power (AUROC and BEDROC values were 0.85 and 1.00, respectively).

Biological evaluation of the tested compounds revealed the highest antiproliferative activities in the group of oxazole-bridged analogues (core 3) with the 3,4,5-trisubstituted phenyl A-ring and 3,4-disubstituted phenyl B-ring. The compounds **23e**, **23f**, **23h**, **23i**, and **24c** (N-methylimidazole-bridged analogue) displayed pronounced cytotoxic activity against the cancer cell lines: A431, HeLa, and MDA-MB-231. Compound **23e** was over 10-fold more potent in inhibiting HeLa cell proliferation with IC_{50} values of 0.009 μM than positive control CA-4. Additionally, the compounds **23a**, **23e**, and **23i** were the most potent inhibitors of tubulin

polymerization determined *in vitro*. Compound **23i**, a sulfur analogue of **23j**, showed 5-fold higher inhibitory effectiveness on tubulin polymerization compared to **23j**. The influence of exchange of oxygen to sulfur could be a promising subject for further studies.

Moreover, compounds **23e** and **23i**, which showed both the highest cytotoxic and antitubulin activities, were further studied in terms of their effect on cell cycle distribution and proapoptotic activity. The impact of **23e** and **23i** on cell proliferation was cell line-dependent. A statistically significant block of the cell cycle at the G2/M phase was observed for compound **23e** in A431, HaCaT, HeLa, MCF-7, MDA-MB-231, SKOV-3 cells, and for compound **23i** in HeLa and SKOV-3 cells. The proapoptotic effect of **23e** and **23i** in studied cell lines was demonstrated with ELISA assay and double staining with Annexin V-FITC/PI. The results of our studies indicate that the CA-4 derivatives **23e** and **23i** may serve as novel lead compounds in research on more effective anticancer agents.

4. Experimental section

4.1. General methods for chemistry

All reagents and solvents were purchased from Sigma-Aldrich, Acros, Fluka, and POCH and were used as received. Reactions that involved air or moisture-sensitive reagents were performed in oven-dried glassware under an inert atmosphere of dry nitrogen with dried solvents, unless otherwise stated. The progress of all reactions was monitored on Merck precoated silica gel plates (with fluorescence indicator UV254) and visualized in UV light (λ_{max} 254 or 365 nm). Melting points were determined in capillary tubes on a Stuart SMP10 micro melting point apparatus and are uncorrected. ^{1}H NMR and ^{13}C NMR spectra were recorded at the Institute of Bioorganic Chemistry, Polish Academy of Sciences in Poznań, using Bruker 400 (400 MHz for ^{1}H and 101 MHz for ^{13}C), Bruker 500 (500 MHz for ^{1}H and 126 MHz for ^{13}C), and Bruker 700

(700 MHz for ^{1}H and 176 MHz for ^{13}C) spectrometers with TMS as an internal standard in $CDCl_3$ or DMSO-d6. Chemical shifts (δ) are quoted in parts per million (ppm) and are referred to as a solvent residual peak ($CDCl_3$, δ 7.26 ppm for ^{1}H and δ 77.0 ppm for ^{13}C NMR; DMSO-d6 δ 2.5 ppm for ^{1}H and δ 39.5 ppm for ^{13}C NMR). Coupling δ constants (J) are quoted in Hertz (Hz) and peaks are listed as singlet (s), doublet (d), triplet (t), multiplet (m), doublet of doublets (dd), triplet of doublets (td), and broad signal (bs). Additional techniques (^{1}H–^{1}H COSY, HSQC, HMBC) were used to assist allocation. LRMS (EI) spectra were recorded on a Bruker 320MS/420GC mass spectrometer and HRMS (EI) spectra were recorded on an Intectra Mass AMD 402 or 604 mass spectrometer by the Advanced Chemical Equipment and Instrumentation Facility at the Faculty of Chemistry, Adam Mickiewicz University in Poznań. IR spectra were recorded on a Bruker FT-IR IFS 66v/s spectrometer by the Advanced Chemical Equipment and Instrumentation Facility at the Faculty of Chemistry, Adam Mickiewicz University in Poznań or on a Thermo Scientific Nicolet iS5 FT-IR spectrometer at the Institute of Mathematical and Natural Sciences, Department of Chemistry, State Higher Vocational School in Tarnów. Dry flash column chromatography was carried out on Merck silica gel 60, particle size 40−63 μm or 15-40 μm using EZSafe low-pressure columns. UV−vis spectra were recorded on a Hitachi UV/vis U-1900 spectrophotometer; λ_{max} (log ε), nm. All final target compounds were characterized and determined to be at least >95% pure using a Waters ACQUITY UPLC H-class system equipped with a UV DAD and TQD Waters MS detector with electrospray ionization at the Department of Medicinal Chemistry, Institute of Pharmacology, Polish Academy of Sciences in Kraków. LC analysis was performed using a ACQUITY UPLC BEH C18 column (2.1 × 50 mm, 1,7 μm) at a flow rate of 0.3 mL/min (20–100% aqueous CH_3CN over 3 min, 100% CH_3CN over 0.5 min, and 100–20% aqueous CH_3CN over 2.5 min).

*4.2. General procedure for synthesis of compounds **1a**, **14a-b**, **15a-b**, **23a-j**, and **24a-f***

*4.2.1. Synthesis of CA-4 (**1a**)*

CA-4 was synthesized according to known procedures [34].

*4.2.1.1. (E)-3-(3-Hydroxy-4-methoxyphenyl)-2-(3,4,5-trimethoxyphenyl)prop-2-enoic acid (**7**)*

A mixture of 3-hydroxy-4-methoxybenzaldehyde **6** (1.36 g, 8.94 mmol), 3,4,5-trimethoxyphenylacetic acid **5** (2.01 g, 8.90 mmol), acetic anhydride (4 mL), and trimethylamine (2 mL) were heated under nitrogen at 110 °C for 4 h. The mixture was cooled and 6 mL of conc. HCl and 6 mL of diluted HCl was added. A yellow solid was obtained which was collected by filtration. It was dissolved in 10% aq NaOH (50 mL) and washed with ethyl acetate (3x5 mL). The organic layers were separated and the aqueous layer was acidified with conc. HCl to pH 3-4. The precipitated crude product was collected by filtration and recrystallized from 70% v/v EtOH with the use of activated carbon to afford **7** as pale yellow crystals. Yield 44% (1.40 g, 3.90 mmol). mp 239-241 °C (lit. [34] 237-239 °C). R_f (EtOAc/n-hexane, 3:1) 0.18. UV-vis (MeOH) λ_{max} (log ε): 322 (4.64), 235 (4.67). HPLC: 95.71%, tR = 2.18 min. ^{1}H NMR (400 MHz, DMSO-d_6) δ 8.94 (bs, 1H, COO**H**), 7.57 (s, 1H, C1a'-**H**), 6.80 (d, J = 8.5 Hz, 1H, C5'-**H**), 6.60 (dd, J = 8.5, 2.0 Hz, 1H, C6'-**H**), 6.53 (d, J = 2.0 Hz, 1H, C2'-**H**), 6.44 (s, 2H, C2-**H**, C6-**H**)), 3.73 (s, 3H, C4-OC**H$_3$**), 3.71 (s, 3H, C4'-OC**H$_3$**), 3.69 (s, 6H, C3-OC**H$_3$**, C5-OC**H$_3$**). ^{13}C NMR (101 MHz, DMSO-d_6) δ 168.57 (**C**OOH), 153.07 (**C3**, **C5**), 148.88 (**C3'**), 145.85 (**C4'**), 139.08 (**C4**), 136.95 (**C1**), 132.14 (**C1'**), 130.33 (**C1a**), 127.03 (**C1a'**), 122.92 (**C6'**), 117.21 (**C2'**), 111.52 (**C5'**), 106.73 (**C2**, **C6**), 60.12 (C4-O**C**H$_3$), 55.94 (C3-O**C**H$_3$, C5-O**C**H$_3$), 55.46 (C4'-O**C**H$_3$). FTIR ATR (KBr) cm^{-1}: 3313 (bs ν O-H), 3073 (ν = C$_{Ar}$-H), 2961 (ν_{as} CH$_3$), 2939 (ν CH$_3$), 2826 (ν O-CH$_3$), 1666 (ν C=O), 1584 (ν C$_{Ar}$=C$_{Ar}$), 1503 (ν C$_{Ar}$=C$_{Ar}$), 1455 (δ_{as} CH$_3$), 1409 (δ_s CH$_3$), 1265 (ν C-O), 1237 ($_{as}$ C$_{Ar}$-O-C), 1123 (ν C-O-C), 1023 (ν_s C$_{Ar}$-O-C), 900 (γ^{oop} OH…O) 805

(γ^{oop} =C_{Ar}-H), 770 (γ^{oop} =C_{Ar}-H), 729 (γ^{oop} = C_{Ar}-H).LRMS (EI) m/z 360.2 ([M]$^+$, 100%). HRMS (EI) calcd for $C_{19}H_{20}O_7$: 360.1204. Found: 360.1241.

*4.2.1.2. (Z)-1-(3-Hydroxy-4-methoxyphenyl)-2-(3,4,5-trimethoxyphenyl)ethene (CA-4, **1a**)*

The obtained *α*-phenylcinnamic acid **7** (1.30 g, 3.60 mmol) was added to powdered copper (1.90 g, 29.90 mmol) in quinoline (15 mL, 16.40 g, 0.13 mol) and the resulting mixture was heated under nitrogen at 200 °C for 3 h. Upon cooling, the mixture was diluted with ethyl acetate (50 mL) and the copper was filtered off. The filtrate was washed with 5% aq HCl (3x20 mL) and the aqueous layer was separated and extracted with ethyl acetate (3x10 mL). The combined organic layers were washed with brine (2x50 mL), dried over $MgSO_4$, filtered, and concentrated under reduced pressure to afford a brown oil which crystallized after a few minutes. The obtained brown solid was dissolved in ethyl acetate (2 mL), purified by flash column chromatography on silica gel (EtOAc/n-hexane, 7:3), and subsequently recrystallized from EtOAc-petroleum ether to give **1a** as colorless crystals. Yield 40% (0.45 g, 1.43 mmol). mp 83-85 °C (lit. [34] 117-118 °C). R_f (EtOAc/n-hexane, 1:1) 0.49. UV-vis (MeOH) λ_{max} (log ε): 298 (3.95). HPLC: 100 %, tR = 3.07 min. ^{1}H NMR (400 MHz, $CDCl_3$) δ 6.92 (d, J = 2.0 Hz, 1H, C2'-**H**), 6.80 (dd, J = 8.3, 1.9 Hz, 1H, C6'-**H**), 6.73 (d, J = 8.3 Hz, 1H, C5'-**H**), 6.53 (s, 2H, C2-**H**, C6-**H**), 6.47 (d, J = 12.2 Hz, 1H, C1a-**H**), 6.41 (d, J = 12.2 Hz, 1H, C1a'-**H**), 5.49 (s, 1H, C3'-O**H**), 3.87 (s, 3H, C4-OC**H$_3$**), 3.84 (s, 3H, C4'-OC**H$_3$**), 3.70 (s, 6H, C3-OC**H$_3$**, C5-OC**H$_3$**).^{13}C NMR (101 MHz, $CDCl_3$) δ 152.82 (**C3**, **C5**), 145.69 (**C3'**), 145.18 (**C4'**), 137.11 (**C4**), 132.64 (**C1**), 130.59 (**C1'**), 129.43 (**C1a**), 128.99 (**C1a'**), 121.06 (**C6'**), 114.98 (**C2'**), 110.25 (**C5'**), 106.00 (**C2**, **C6**), 60.87 (C4-O**C**H$_3$), 55.90 (C4'-O**C**H$_3$), 55.88 (C3-O**C**H$_3$, C5-O**C**H$_3$). FTIR ATR (KBr) cm^{-1}: 3382 (ν O-H), 3068 (ν =C_{Ar}-H), 3041 (ν =C_{Ar}-H), 3010 (ν =C_{ethene}-H), 2934 (νCH$_3$), 2972 (ν_{as} CH$_3$), 2833 (νO-CH$_3$), 1579 (νC_{Ar}=C_{Ar}), 1511 (νC_{Ar}=C_{Ar}),

1455 (δ_{as} CH_3), 1400 (δ_s CH_3), 1274 (ν_{as} C_{Ar}-O-C), 1222 (ν C_{Ar}-OH), 1133 (ν C-O-C), 1036 (ν_s C_{Ar}-O-C), 975 (γ^{oop} =C_{ethene}-H), 877 (γ^{oop} =C_{Ar}-H) 793 (γ^{oop} =C_{Ar}-H), 761 (γ^{oop} =C_{Ar}-H). LRMS (EI) m/z 315.9 ($[M]^+$, 100%). HRMS (EI) m/z calcd for $C_{18}H_{20}O_5$: 316.1305. Found: 316.1311.

*4.2.2. General procedure for compounds **14a** and **14b** (α-phenylcinnamic acids, core 1)*

A mixture of benzaldehydes **11d** and **13** (3 mmol), 3,4,5-trimethoxyphenylacetic acid **5** (0.68 g, 3 mmol), acetic anhydride (2 mL), and trimethylamine (2 mL) were heated under nitrogen at 115 °C for 4 h. The mixture was cooled and 5% aq HCl (30 mL) was added. A yellow solid was obtained which was collected by filtration. It was dissolved in 10% aq NaOH (50 mL) and washed with ethyl acetate (3x20 mL). The organic layers were separated and the aqueous layer was acidified with 5% aq HCl to pH 3-4. The precipitated crude product was collected by filtration, washed with water and recrystallized from the isopropanol/water mixture (1:1, 40 mL) to afford *α*-phenylcinammic acid derivatives **14a-b** as pale yellow crystals**.**

*4.2.2.1. (E)-3-(3-Methoxy-2-methylthiophenyl)-2-(3,4,5-trimethoxyphenyl)prop-2-enoic acid (**14a**)*

Pale yellow crystals. Yield 34% (0.40 g, 1.02 mmol). mp 178-180 °C. R_f ($CHCl_3$/MeOH, 10:1) 0.44. UV-vis (MeOH) λ_{max} (log ε): 288 (3.87). HPLC: 97.24 %, tR = 2.79 min. ^{1}H NMR (500 MHz, $CDCl_3$) δ 8.46 (s, 1H, C1a'-**H**), 6.99 (t, *J* = 8.0 Hz, 1H, C5'-**H**), 6.77 (d, *J* = 8.2 Hz, 1H, C6'-**H**), 6.47 (d, *J* = 7.8 Hz, 1H, C4'-**H**), 6.38 (s, 2H, C2-**H**, C6-**H**), 3.91 (s, 3H, C4-OC**H$_3$**), 3.83 (s, 3H, C3'-OC**H$_3$**), 3.69 (s, 6H, C3-OC**H$_3$**, C5-OC**H$_3$**), 2.42 (s, 3H, C2'-SC**H$_3$**). ^{13}C NMR (126 MHz, $CDCl_3$) δ 172.36 (**C**OOH), 159.75 (**C3'**), 152.95 (**C3**, **C5**), 141.97 (**C1a'**), 139.48 (**C4**), 137.71 (**C1'**), 132.30 (**C1a**), 129.88 (**C2'**), 128.52 (**C5'**), 125.12 (**C1**), 122.56 (**C6'**), 110.82 (**C4'**), 107.52 (**C2**, **C6**), 60.87 (C4-O**C**H_3), 56.04 (C3-O**C**H_3, C5-O**C**H_3), 55.93 (C3'-O**C**H_3), 18.41 (C2'-S**C**H_3). FTIR ATR (KBr) cm^{-1}: 3068 (ν=C_{Ar}-H), 2958 (ν_{as} CH_3), 2932 (bs ν

O-H), 2851 (ν_s CH_3), 2832 (νO-CH_3), 1682 (νC=O), 1578 ($\nu$$C_{Ar}$=$C_{Ar}$), 1506 ($\nu$$C_{Ar}$=$C_{Ar}$), 1454 ($\delta_{as}$ CH_3), 1407 (δ_s CH_3), 1265 (νC-O), 1237 (ν_{as} C_{Ar}-O-C), 1125 (νC-O-C), 1065 (ν_s C_{Ar}-O-C), 967 (γ^{oop} =C_{ethene}-H), 795 (γ^{oop} =C_{Ar}-H), 741 (γ^{oop} =C_{Ar}-H), 724 (γ^{oop} =C_{Ar}-H). LRMS (EI) m/z 390.1 ($[M]^+$, 58.5%), 325.1 (100%). HRMS (EI) m/z calcd for $C_{20}H_{22}O_6S$: 390.1132. Found: 390.1149.

*4.2.2.2. (E)-3-(2-Methylthiophenyl)-2-(3,4,5-trimethoxyphenyl)prop-2-enoic acid (**14b**)*

Pale yellow crystals. Yield 40% (0.43 g, 1.19 mmol). mp 190-192 °C. R_f ($CHCl_3$/MeOH, 10:1) 0.43. UV-vis (MeOH) λ_{max} (log ε): 268 (4.04). HPLC: 100 %, tR = 2.88 min. ^{1}H NMR (500 MHz, $CDCl_3$) δ 8.23 (s, 1H, C1a'-**H**), 7.26 (d, J = 7.2 Hz, 1H, C3'-**H**), 7.20 (t, J = 8.3 Hz, 1H, C4'-**H**), 6.87 (t, J = 7.9 Hz, 1H, C5'-**H**), 6.79 (d, J = 7.3 Hz, 1H, C6'-**H**), 6.40 (s, 2H, C2-**H**, C6-**H**), 3.84 (s, 3H, C4-OC**H$_3$**), 3.69 (s, 6H, C3-OC**H$_3$**, C5-OC**H$_3$**), 2.53 (s, 3H, C2'-SC**H$_3$**). ^{13}C NMR (126 MHz, $CDCl_3$) δ 172.22 (**C**OOH), 153.02 (**C3**, **C5**), 140.00 (**C2'**), 139.45 (**C1a'**), 137.81 (**C4**), 133.69 (**C1a**), 132.83 (**C1'**), 129.89 (**C3'**), 129.78 (**C1**), 129.25 (**C6'**), 125.96 (**C4'**), 124.76 (**C5'**), 107.41 (**C2**, **C6**), 60.87 (C4-O**C**H_3), 56.04 (C3-O**C**H_3, C5-O**C**H_3), 16.32 (C2'-S**C**H_3). FTIR ATR (KBr) cm^{-1}: 3062 (ν=C_{Ar}-H), 2965 (ν_{as} CH_3), 2924 (bs νO-H), 2829 (ν O-CH_3), 1684 (ν C=O), 1582 (ν C_{Ar}=C_{Ar}), 1507 (ν C_{Ar}=C_{Ar}), 1454 (δ_{as} CH_3), 1409 (δ_s CH_3), 1261 (ν C-O), 1238 (ν_{as} C_{Ar}-O-C), 1125 (ν C-O-C), 1066 (ν_s C_{Ar}-O-C), 898 (γ^{oop} =C_{Ar}-H), 834 (γ^{oop} =C_{Ar}-H), 740 (γ^{oop} =C_{Ar}-H). LRMS (EI) m/z 360.1 ($[M]^+$, 100%), 295.1 (93.3%). HRMS (EI) m/z calcd for $C_{19}H_{20}O_5S$: 360.1026. Found: 360.1055.

*4.2.3. General procedure for compounds **15a** and **15b** ((Z)-stilbene, core 2)*

α-Phenylcinnamic acids **14a-b** (0.80 mmol) were added to powdered copper (0.42 g, 6.64 mmol) in quinoline (3.5 mL, 3.23 g, 25 mmol) and the resulting mixture was heated under

nitrogen at 200 °C for 2.5 h. Upon cooling, the mixture was diluted with ethyl acetate (30 mL) and the copper was filtered off. The filtrate was washed with 5% aq HCl (3x20 mL) and the aqueous layer was separated and extracted with ethyl acetate (3x10 mL). The combined organic layers were washed with brine (3x20 mL), dried over $MgSO_4$, filtered, and concentrated under reduced pressure to afford brown oils. The residue was dissolved in ethyl acetate (2 mL) and purified by flash column chromatography on silica gel (EtOAc/n-hexane, 10:1) to afford pure products **15a-b** as white solids.

*4.2.3.1. (Z)-1-(3-Methoxy-2-methylthiophenyl)-2-(3,4,5-trimethoxyphenyl)ethene (**15a**)*

White solid. Yield 40% (0.11 g, 0.32 mmol). mp 78-80 °C. R_f (EtOAc/n-hexane, 10:1) 0.67. UV-vis (MeOH) λ_{max} (log ε): 288 (4.15). HPLC: 98.85 %, tR = 3.50 min. ^{1}H NMR (500 MHz, $CDCl_3$) δ 7.14 (t, J = 7.7 Hz, 1H, C5'-**H**), 6.90 (d, J = 8.2 Hz, 1H, C6'-**H**), 6.87 (d, J = 12.1 Hz, 1H, C1a'-**H**), 6.79 (d, J = 8.2 Hz, 1H, C4'-**H**), 6.54 (d, J = 12.1 Hz, 1H, C1a-**H**), 6.37 (s, 2H, C2-**H**, C6-**H**), 3.92 (s, 3H, C4-OC**H$_3$**), 3.80 (s, 3H, C3'-OC**H$_3$**), 3.60 (s, 6H, C3-OC**H$_3$**, C5-OC**H$_3$**), 2.36 (s, 3H, C2'-SC**H$_3$**). ^{13}C NMR (126 MHz, $CDCl_3$) δ 160.01 (**C3'**), 152.63 (**C3**, **C5**), 142.98 (**C4**), 137.14 (**C1'**), 132.11 (**C2'**), 129.96 (**C1a'**), 129.41 (**C1a**), 128.68 (**C5'**), 123.45 (**C1**), 122.49 (**C6'**), 109.58 (**C4'**), 106.22 (**C2**, **C6**), 60.84 (C4-O**C**H$_3$), 55.95 (C3'-O**C**H$_3$), 55.71 (C3-O**C**H$_3$, C5-O**C**H$_3$), 18.17 (C2'-S**C**H$_3$). FTIR ATR (KBr) cm^{-1}: 3117 (ν =C_{Ar}-H), 3055 (ν =C_{Ar}-H), 3010 (ν=C_{ethene}-H), 2967 (ν_{as} CH_3), 2942 ($\nu$$CH_3$), 2825 ($\nu$O-$CH_3$), 1581 ($\nu$$C_{Ar}$=$C_{Ar}$), 1507 ($\nu$$C_{Ar}$=$C_{Ar}$), 1467 ($\delta_{as}$ CH_3), 1396 (δ_s CH_3), 1252 (ν_{as} C_{Ar}-O-C), 1119 (νC-O-C), 1064 (ν_s C_{Ar}-O-C), 964 (γ^{oop} =C_{ethene}-H), 838 (γ^{oop} =C_{Ar}-H) 780 (γ^{oop} =C_{Ar}-H), 722 (γ^{oop} =C_{Ar}-H). LRMS (EI) m/z 346.1 ([M]$^+$, 100%). HRMS (EI) m/z calcd for $C_{19}H_{20}O_5S$: 346.1233. Found: 346.1211.

*4.2.3.2. (Z)-1-(2-Methylthiophenyl)-2-(3,4,5-trimethoxyphenyl)ethene (**15b**)*

White solid. Yield 40% (0.10 g, 0.32 mmol). mp 73-75 °C. R_f (EtOAc/n-hexane, 10:1) 0.68. UV-vis (MeOH) λ_{max} (log ε): 266 (3.92). HPLC: 95.70 %, tR = 3.60 min. ^{1}H NMR (400 MHz, $CDCl_3$) δ 7.26 – 7.18 (m, 3H, C3'-**H**, C4'-**H**, C6'-**H**), 7.08 – 7.02 (m, 1H, C5'-**H**), 6.64 (d, J = 12.0 Hz, 1H, C1a'-**H**), 6.56 (d, J = 12.0 Hz, 1H, C1a-**H**), 6.37 (s, 2H, C2-**H**, C6-**H**), 3.80 (s, 3H, C4-OC**H$_3$**), 3.59 (s, 6H, C3-OC**H$_3$**, C5-OC**H$_3$**), 2.47 (s, 3H, C2'-SC**H$_3$**). ^{13}C NMR (101 MHz, $CDCl_3$) δ 152.66 (**C3**, **C5**), 137.68 (**C2'**), 137.27 (**C4**), 136.54 (**C1'**), 131.92 (**C1**), 131.29 (**C3'**), 129.48 (**C1a**), 127.85 (**C6'**), 127.66 (**C1a'**), 125.26 (**C4'**), 124.69 (**C5'**), 106.15 (**C2**, **C6**), 60.83 (C4-O**C**H$_3$), 55.70 (C3-O**C**H$_3$, C5-O**C**H$_3$), 15.61 (C2'-S**C**H$_3$). FTIR ATR (KBr) cm^{-1}: 3076 (ν =C_{Ar}-H), 3056 (ν=C_{Ar}-H), 3010 (ν=C_{ethene}-H), 2959 (ν_{as} CH_3), 2936 (ν CH_3), 2836 (ν O-CH_3), 1580 (ν C_{Ar}=C_{Ar}), 1506 (ν C_{Ar}=C_{Ar}), 1450 (δ_{as} CH_3), 1399 (δ_s CH_3), 1236 (ν_{as} C_{Ar}-O-C), 1126 (ν C-O-C), 1013 (ν_s C_{Ar}-O-C), 961 (γ^{oop} =C_{ethene}-H), 868 (γ^{oop} =C_{Ar}-H) 852 (γ^{oop} =C_{Ar}-H), 745 (γ^{oop} =C_{Ar}-H). LRMS (EI) m/z 316.1 ([M]$^+$, 100%). HRMS (EI) m/z calcd for $C_{19}H_{20}O_5S$: 316.1128. Found: 316.1137.

*4.2.4. General procedure for compounds **23a-b**, **23d**, **23f-j** (oxazole-bridged analogues, core 3)*

A mixture of appropriate tosylmethyl isocyanide (TosMIC) **20-22** (1.2 mmol), benzaldehyde **6a-d**, **8d**, **9d**, **13** (1 mmol), and anhydrous potassium carbonate (0.33 g, 2.4 mmol) in 10 mL of methanol and 3 mL of DME was refluxed under nitrogen for 2 h. After it was cooled to room temperature, water was added (30 mL) and the solution was extracted with ethyl acetate (3x20 mL). The combined organic layers were washed with brine (100 mL), dried over $MgSO_4$, filtered, and concentrated under reduced pressure. The residue was purified by recrystallization from isopropanol (15 mL) with the use of activated carbon **23f-j** or by flash column chromatography on silica gel (EtOAc/n-hexane, 1:1) **23a-b**, **23d**.

*4.2.4.1. 4-(3,4,5-Trimethoxyphenyl)-5-(2-methylthiophenyl)oxazole (**23a**)*

Pale yellow crystals. Yield 45% (0.16 g, 0.45 mmol). mp 87-89 °C. R_f (EtOAc/n-hexane, 1:1) 0.5. UV-vis (MeOH) λ_{max} (log ε): 244 (4.29). HPLC: 98.50%, tR = 3.24 min.^{1}H NMR (400 MHz, $CDCl_3$) δ 8.00 (s, 1H, C2ox-**H**), 7.49 – 7.43 (m, 1H, C4'-**H**), 7.38 (dd, *J* = 7.6, 1.5 Hz, 1H, C6'-**H**), 7.35 (d, *J* = 7.3 Hz, 1H, C3'-**H**), 7.23 (td, *J* = 7.5, 1.2 Hz, 1H, C5'-**H**), 6.80 (s, 2H, C2-**H**, C6-**H**), 3.82 (s, 3H, C4-OC**H$_3$**), 3.66 (s, 6H, C3-OC**H$_3$**, C5-OC**H$_3$**), 2.40 (s, 3H, C2'-SC**H$_3$**). ^{13}C NMR (101 MHz, $CDCl_3$) δ 153.09 (**C3**, **C5**), 150.17 (**C2ox**), 143.75 (**C5ox**), 140.98 (**C4**), 137.57(**C4ox**), 135.88 (**C2'**), 131.54 (**C4'**), 130.61 (**C6'**), 127.68 (**C1**), 126.61 (**C1'**), 125.57 (**C3'**), 124.85 (**C5'**), 103.35 (**C2**, **C6**), 60.80 (C4-O**C**H$_3$), 55.69 (C3-O**C**H$_3$, C5-O**C**H$_3$), 15.61 (C2'-S**C**H$_3$). FTIR ATR (KBr) cm^{-1}: 3109 (νN=C$_{Ar}$-H), 3067 (ν=C$_{Ar}$-H), 2998 (νCH$_3$), 2955 (ν_{as} CH$_3$), 2933 (νCH$_3$), 2837 (νO-CH$_3$), 1622 (νC$_{Ar}$=N), 1586 (νC$_{Ar}$=C$_{Ar}$), 1519 (νC$_{Ar}$=C$_{Ar}$), 1459 (δ_{as} CH$_3$), 1372 (δ_s CH$_3$), 1241 (ν_{as} C$_{Ar}$-O-C), 1125 (νC-O-C), 1049 (ν_s C$_{Ar}$-O-C), 845 (γ^{oop} =C$_{Ar}$-H), 759 (γ^{oop} =C$_{Ar}$-H). LRMS (EI) m/z 357.3 ([M]$^+$, 100%). HRMS (EI) m/z calcd for $C_{19}H_{19}NO_4S$: 357.1029. Found: 357.1040.

*4.2.4.2. 4-(3,4,5-Trimethoxyphenyl)-5-(4-methoxy-3-N,N-dimethylcarbamoylthiophenyl)oxazole (**23b**)*

White crystals. Yield 36% (0.16 g, 0.36 mmol). mp 123-124 °C. R_f (EtOAc/n-hexane, 3:1) 0.39. UV-vis (MeOH) λ_{max} (log ε): 294 (4.09), 242 (4.25). HPLC: 100%, tR = 2.95 min. ^{1}H NMR (500 MHz, $CDCl_3$) δ 7.90 (s, 1H, C2ox-**H**), 7.81 (d, *J* = 2.3 Hz, 1H, C2'-**H**), 7.70 (dd, *J* = 8.7, 2.3 Hz, 1H, C6'-**H**), 6.99 (d, J = 8.7 Hz, 1H, C5'-**H**), 6.93 (s, 2H, C2-**H**, C6-**H**), 3.91 (s, 3H, C4-OC**H$_3$**), 3.88 (s, 3H, C4'-OC**H$_3$**), 3.80 (s, 6H, C3-OC**H$_3$**, C5-OC**H$_3$**), 3.11 (s, 3H, C8'**H$_3$**), 2.99 (s, 3H, C9'**H$_3$**). ^{13}C NMR (126 MHz, $CDCl_3$) δ 165.49 (**C7'**), 160.48 (**C4'**), 153.35 (**C3**, **C5**), 149.31 (**C2ox**), 144.73 (**C5ox**), 137.85 (**C4**), 136.46 (**C2'**), 133.78 (**C4ox**), 130.18 (**C6'**), 127.50

(**C1**), 121.57 (**C1**'), 117.59 (**C3'**), 111.48 (**C5'**), 104.71 (**C2**, **C6**), 60.92 (C4-O**C**H_3), 56.28 (C4'-O**C**H_3), 56.13, (C3-O**C**H_3, C5-O**C**H_3), 36.97 (**C8'**), 36.95 (**C9'**). FTIR ATR (KBr) cm^{-1}: 3121 (ν N=C_{Ar}-H), 3009 (ν=C_{Ar}-H), 2968 (ν_{as} CH_3), 2935 (νCH_3), 2836 (νO-CH_3), 1670 (νC=O), 1580 (νC_{Ar}=C_{Ar}), 1507 (νC_{Ar}=C_{Ar}), 1461 (δ_{as} CH_3), 1366 (δ_s CH_3), 1270 (νC-N), 1238 (ν_{as} C_{Ar}-O-C), 1126 (ν C-O-C), 1067 (ν_s C_{Ar}-O-C), 821 (γ^{oop} =C_{Ar}-H), 728 (γ^{oop} =C_{Ar}-H). LRMS (EI) m/z 444.1 ($[M]^+$, 100%), 72.1 ($[(CH_3)_2NCO]^+$, 97.4%). HRMS (EI) m/z calcd for $C_{22}H_{24}N_2O_6S$: 444.1350. Found: 444.1338.

*4.2.4.3. 4-(3,5-Dimethoxy-4-methylthiophenyl)-5-(4-methoxy-3-N,N-dimethylthiocarbamoyloxy-phenyl)oxazole (**23d**)*

White crystals. Yield 51% (0.23 g, 0.51 mmol). mp 129-132 °C. R_f (EtOAc/n-hexane, 1:1) 0.35. UV-vis (MeOH) λ_{max} (log ε): 300 (4.24), 244 (4.45). HPLC: 96.79%, tR = 3.25 min. ^{1}H NMR (500 MHz, $CDCl_3$) δ 7.92 (s, 1H, C2ox-**H**), 7.53 (dd, J = 8.6, 2.2 Hz, 1H, C6'-**H**), 7.35 (d, J = 2.2 Hz, 1H, C2'-**H**), 7.00 (d, J = 8.6 Hz, 1H, C5'-**H**), 6.92 (s, 2H, C2-**H**, C6-**H**), 3.86 (s, 3H, C4'-OC**H$_3$**), 3.85 (s, 6H, C3-OC**H$_3$**, C5-OC**H$_3$**), 3.44 (s, 3H, C8'**H$_3$**), 3.34 (s, 3H, C9'**H$_3$**), 2.40 (s, 3H, C4-SC**H$_3$**). ^{13}C NMR (126 MHz, $CDCl_3$) δ 187.30 (**C7'**), 160.54 (**C3**, **C5**), 152.30 (**C4'**), 149.41 (**C2ox**), 145.38 (**C5ox**), 142.90 (**C3'**), 133.80 (**C4ox**), 132.99 (**C1**), 125.89 (**C6'**), 122.80 (**C2'**), 121.10 (**C1**'), 112.57 (**C5'**), 111.96 (**C4**), 103.61 (**C2**, **C6**), 56.34 (C3-O**C**H_3, C5-O**C**H_3), 56.08 (C4'-O**C**H_3), 43.44 (**C8'**), 38.75 (**C9'**), 17.82 (C4-S**C**H_3). FTIR ATR (KBr) cm^{-1}: 3105 (ν N=C_{Ar}-H), 3024 (ν=C_{Ar}-H), 2994 (νCH_3), 2951 (ν_{as} CH_3), 2926 (νCH_3), 2855 (νO-CH_3), 1559 (νC_{Ar}=C_{Ar}), 1510 (νC_{Ar}=C_{Ar}), 1463 (δ_{as} CH_3), 1406 (δ_s CH_3), 1270 (νC-N), 1236 (ν_{as} C_{Ar}-O-C), 1124 (νC-O-C), 1025 (ν_s C_{Ar}-O-C), 832 (γ^{oop} =C_{Ar}-H), 772 (γ^{oop} =C_{Ar}-H). LRMS (EI) m/z 460.1 ($[M]^+$, 58%), 88 ($[(CH_3)_2NCS]^+$, 100%). HRMS (EI) m/z calcd for $C_{22}H_{24}N_2O_5S_2$: 460.1121. Found: 460.1140.

*4.2.4.4. 4-(3,4,5-Trimethoxyphenyl)-5-(3-methoxy-4-methylthiophenyl)oxazole (**23f**)*

White crystals. Yield 59% (0.23 g, 0.59 mmol). mp 114-116 °C. R_f (EtOAc/n-hexane, 1:1) 0.39. UV-vis (MeOH) λ_{max} (log ε): 320 (4.20). HPLC: 98.35%, tR = 3.34 min. ^{1}H NMR (500 MHz, $CDCl_3$) δ 7.93 (s, 1H, C2ox-**H**), 7.28 (dd, J = 8.1, 1.8 Hz, 1H, C6'-**H**), 7.12 (d, J = 8.1 Hz, 1H, C5'-**H**), 7.09 (d, J = 1.7 Hz, 1H, C2'-**H**), 6.92 (s, 2H, C2-**H**, C6-**H**), 3.88 (s, 3H, C3'-OC**H$_3$**), 3.83 (s, 3H, C4-OC**H$_3$**), 3.80 (s, 6H, C3-OC**H$_3$**, C5-OC**H$_3$**), 2.45 (s, 3H, C4'-SC**H$_3$**). ^{13}C NMR (126 MHz, $CDCl_3$) δ 155.89 (**C3'**), 153.33 (**C3**, **C5**), 149.36 (**C2ox**), 145.40 (**C5ox**), 138.07 (**C4**), 134.38 (**C4ox**), 128.69 (**C1**), 127.55 (**C4'**), 125.84 (**C1**'), 125.17 (**C5'**), 119.72 (**C6'**), 108.08 (**C2'**), 105.12 (**C2**, **C6**), 60.94 (C4-O**C**H$_3$), 56.14 (C3-O**C**H$_3$, C5-O**C**H$_3$), 55.84 (C3'-O**C**H$_3$), 14.38 (C4'-S**C**H$_3$). FTIR ATR (KBr) cm^{-1}: 3106 (ν N=C_{Ar}-H), 3004 (ν =C_{Ar}-H), 2952 (ν_{as} CH_3), 2934 (ν CH_3), 2837 (ν O-CH_3), 1577 (ν C_{Ar}=C_{Ar}), 1515 (ν C_{Ar}=C_{Ar}), 1463 (δ_{as} CH_3), 1369 (δ_s CH_3), 1234 (ν_{as} C_{Ar}-O-C), 1130 (ν C-O-C), 1060 (ν_s C_{Ar}-O-C), 835 (γ^{oop} =C_{Ar}-H). LRMS (EI) m/z 387.1 ([M]$^+$, 100%). HRMS (EI) m/z calcd for $C_{20}H_{21}NO_5S$: 387.1135. Found: 387.1155.

*4.2.4.5. 4-(3,4,5-Trimethoxyphenyl)-5-(3-bromo-5-methoxy-4-methylthiophenyl)oxazole (**23g**)*

Pale yellow crystals. Yield 49% (0.23 g, 0.49 mmol). mp 112-114 °C. R_f (EtOAc/n-hexane, 1:1) 0.37. UV-vis (MeOH) λ_{max} (log ε): 322 (4.32). HPLC: 100%, tR = 3.69 min. ^{1}H NMR (500 MHz, $CDCl_3$) δ 7.95 (s, 1H, C2ox-**H**), 7.64 (d, J = 1.7 Hz, 1H, C2'-**H**), 7.10 (d, J = 1.7 Hz, C6'-**H**), 6.92 (s, 2H, C2-**H**, C6-**H**), 3.89 (s, 3H, C5'-OC**H$_3$**), 3.83 (s, 6H, C3-OC**H$_3$**, C5-OC**H$_3$**), 3.82 (s, 3H, C4-OC**H$_3$**), 2.43 (s, 3H, C4'-SC**H$_3$**). ^{13}C NMR (126 MHz, $CDCl_3$) δ 160.69 (**C5'**), 153.45 (**C3**, **C5**), 149.88 (**C2ox**), 143.64 (**C5ox**), 138.50 (**C4**), 135.99 (**C3'**), 130.27 (**C4ox**), 129.96 (**C1**), 126.90 (**C4'**), 126.56 (**C1**'), 122.97 (**C2'**), 108.01 (**C6'**), 105.26 (**C2**, **C6**), 60.97 (C4-O**C**H$_3$), 56.32 (C5'-O**C**H$_3$), 56.22 (C3-O**C**H$_3$, C5-O**C**H$_3$), 18.24 (C4'-S**C**H$_3$). FTIR ATR (KBr)

cm^{-1}: 3109 (νN=C_{Ar}-H), 3010 (ν=C_{Ar}-H), 2980 (ν_{as} CH_3), 2924 (νCH_3), 2825 (νO-CH_3), 1586 (νC_{Ar}=C_{Ar}), 1528 (νC_{Ar}=C_{Ar}), 1469 (δ_{as} CH_3), 1391 (δ_s CH_3), 1245 (ν_{as} C_{Ar}-O-C), 1124 (νC-O-C), 1029 (ν_s C_{Ar}-O-C), 828 (γ^{oop} =C_{Ar}-H), 731 (γ^{oop} =C_{Ar}-H). LRMS (EI) m/z 465.1 ($[M]^+$, 100%), 467.1 ($[M^+ + 2]$, 93,6%). HRMS (EI) m/z calcd for $C_{20}H_{20}BrNO_5S$: 465.0240. Found: 465.0249.

*4.2.4.6. 4-(3-Bromo-4,5-dimethoxyphenyl)-5-(3-methoxy-4-methylthiophenyl)oxazole (**23h**)*

Pale yellow crystals. Yield 62% (0.27 g, 0.62 mmol). mp 102-105 °C. R_f (EtOAc/n-hexane, 1:1) 0.53. UV-vis (MeOH) λ_{max} (log ε): 322 (4.50). HPLC: 100%, tR = 3.70 min. ^{1}H NMR (500 MHz, $CDCl_3$) δ 7.93 (s, 1H, C2ox-**H**), 7.50 (d, *J* = 2.0 Hz, 1H, C2-**H**), 7.24 (d, *J* = 1.7 Hz, 1H, C2'-**H**), 7.21 (d, *J* = 2.0 Hz, 1H, C6-**H**), 7.14 (d, *J* = 8.1 Hz, 1H, C5'-**H**), 7.09 (d, *J* = 1.7 Hz, 1H, C6'-**H**), 3.89 (s, 3H, C5-OC**H$_3$**), 3.84 (s, 3H, C3'-OC**H$_3$**), 3.83 (s, 3H, C4-OC**H$_3$**), 2.47 (s, 3H, C4'-SC**H$_3$**). ^{13}C NMR (126 MHz, $CDCl_3$) δ 155.93 (**C5**), 153.71 (**C3'**), 149.49 (**C2ox**), 146.37 (**C5ox**), 145.86 (**C4**), 132.90 (**C4ox**), 129.25 (**C1**), 129.12 (**C4'**), 125.42 (**C1'**), 125.30 (**C2**), 124.02 (**C5'**), 119.63 (**C6'**), 117.66 (**C3**), 111.45 (**C6**), 107.88 (**C2'**), 60.68 (C4-O**C**H_3), 56.13 (C3'-O**C**H_3), 55.90 (C5-O**C**H_3), 14.34 (C4'-S**C**H_3). FTIR ATR (KBr) cm^{-1}: 3131 (νN=C_{Ar}-H), 3002 (ν =C_{Ar}-H), 2959 (ν_{as} CH_3), 2932 (νCH_3), 2830 (ν O-CH_3), 1562 (ν C_{Ar}=C_{Ar}), 1513 (ν C_{Ar}=C_{Ar}), 1461 (δ_{as} CH_3), 1361 (δ_s CH_3), 1262 (ν_{as} C_{Ar}-O-C), 1043 (ν_s C_{Ar}-O-C), 850 (γ^{oop} =C_{Ar}-H). LRMS (EI) m/z 435.1 ($[M]^+$, 97.1%), 437.0 ($[M^+ + 2]$, 100%) HRMS (EI) m/z calcd for $C_{19}H_{18}BrNO_4S$: 435.0134. Found: 435.0155.

*4.2.4.7. 4-(3-Bromo-4,5-dimethoxyphenyl)-5-(4-methoxy-3-methylthiophenyl)oxazole (**23i**)*

Pale yellow crystals. Yield 57% (0.25 g, 0.57 mmol). mp 102-105 °C. R_f (EtOAc/n-hexane, 1:1) 0.53. UV-vis (MeOH) λ_{max} (log ε): 294 (4.16). HPLC: 99.03%, tR = 3.75 min. ^{1}H NMR (500 MHz, $CDCl_3$) δ 7.91 (s, 1H, C2ox-**H**), 7.48 (d, *J* = 2.0 Hz, 1H, C2-**H**), 7.41 (dd, *J* = 8.4, 2.1

Hz, 1H, C6'-**H**), 7.38 (d, *J* = 2.1 Hz, 1H, C2'-**H**), 7.19 (d, *J* = 1.9 Hz, 1H, C6-**H**), 6.86 (d, *J* = 8.5 Hz, 1H, C5'-**H**), 3.94 (s, 3H, C5-OC**H$_3$**), 3.88 (s, 3H, C4-OC**H$_3$**), 3.81 (s, 3H, C4'-OC**H$_3$**), 2.33 (s, 3H, C3'-SC**H$_3$**). ^{13}C NMR (126 MHz, $CDCl_3$) δ 156.59 (**C5**), 153.66 (**C4'**), 149.36 (**C2ox**), 146.27 (**C5ox**), 145.90 (**C4**), 132.25 (**C4ox**), 129.34 (**C1**), 128.12 (**C1'**), 124.57 (**C2**), 123.91 (**C5'**), 124.57 (**C6'**), 121.41 (**C3'**), 117.74 (**C3**), 111.27 (**C6**), 109.96 (**C2'**), 60.67 (C4-O**C**H_3), 56.10 (C4'-O**C**H_3), 55.98 (C5-O**C**H_3), 14.37 (C3'-S**C**H_3). FTIR ATR (KBr) cm^{-1}: 3112 (ν N=C_{Ar}-H), 3008 (ν =C_{Ar}-H), 2997 (ν CH_3), 2942 (ν CH_3), 2836 (ν O-CH_3), 1565 (ν C_{Ar}=C_{Ar}), 1523 (ν C_{Ar}=C_{Ar}), 1495 (δ_{as} CH_3), 1357 (δ_s CH_3), 1248 (ν_{as} C_{Ar}-O-C), 1045 (ν_s C_{Ar}-O-C), 848 (γ^{oop} =C_{Ar}-H). LRMS (EI) m/z 435.1 ([M]$^+$, 98%), 437.0 ([M$^+$ + 2], 100%) HRMS (EI) m/z calcd for $C_{19}H_{18}BrNO_4S$: 435.0134. Found: 435.0120.

*4.2.4.8. 4-(3-Bromo-4,5-dimethoxyphenyl)-5-(3,4-dimethoxyphenyl)oxazole (**23j**)*

White solid. Yield 45% (0.19 g, 0.45 mmol). mp 111-112 °C. R_f (EtOAc/n-hexane, 1:1) 0.51. UV-vis (MeOH) λ_{max} (log ε): 298 (4.10). HPLC: 98.53%, tR = 3.44 min. ^{1}H NMR (400 MHz, $CDCl_3$) δ 7.91 (s, 1H, C2ox-**H**), 7.50 (d, J = 1.9 Hz, 1H, C2-**H**), 7.22 (td, J = 4.2, 2.1 Hz, 2H, C2'-**H**, C6'-**H**), 7.14 (d, J = 2.0 Hz, 1H, C6-**H**), 6.91 (d, J = 8.4 Hz, 1H, C5'-**H**), 3.93 (s, 3H, C5-OC**H$_3$**), 3.88 (s, 3H, C4-OC**H$_3$**), 3.82 (s, 6H, C3'-OC**H$_3$**, C4'-OC**H$_3$**). ^{13}C NMR (101 MHz, $CDCl_3$) δ 153.66 (**C3'**), 149.82 (**C5**), 149.30 (**C2ox**), 149.03 (**C4'**), 146.23 (**C4**), 146.09 (**C5ox**), 132.14 (**C1**), 129.33 (**C3**), 123.88 (**C2**), 120.89 (**C1'**), 120.00 (**C6'**), 117.64 (**C4ox**), 111.28 (**C2'**), 111.23 (**C5'**), 109.86 (**C6**), 60.67 (C4-O**C**H_3), 56.09 (C5-O**C**H_3), 55.96 (C3'-O**C**H_3), 55.94 (C4'-O**C**H_3). FTIR ATR (KBr) cm^{-1}: 3117 (νN=C_{Ar}-H), 3007 (ν =C_{Ar}-H), 2945 (ν CH_3), 2837 (ν O-CH_3), 1558 (ν C_{Ar}=C_{Ar}), 1513 (ν C_{Ar}=C_{Ar}), 1486 (δ_{as} CH_3), 1359 (δ_s CH_3), 1228 (ν_{as} C_{Ar}-O-C), 1126 (ν C-O-C), 1026 (ν_s C_{Ar}-O-C), 839 (γ^{oop} =C_{Ar}-H), 652 (γ^{oop} =C_{Ar}-H). LRMS (EI)

m/z 419.2 ([M]$^+$, 100%), 421.3 ([M$^+$ + 2], 99,9%); HRMS (EI) m/z calcd for $C_{19}H_{18}BrNO_5$: 419.0368. Found: 419.0383.

*4.2.5. General procedure for compounds **23c** and **23e** (oxazole-bridged analogues, core 3)*

A mixture of **23a** or **23d** (0.28 g, 0.63 mmol), 10% KOH/MeOH (10 mL) was heated at 80 °C under nitrogen for 2 h. Upon cooling mixture was diluted with water (20 mL) and solution was acidified with 5% aq HCl to pH 3-4. The resulting suspension was extracted with ethyl acetate (3x20 mL). The combined organic layers were washed with brine (100 mL), dried over $MgSO_4$, filtered and concentrated under reduced pressure. The residue was purified by recrystallization from isopropanol (15 mL) **23c** or isopropanol/petroleum ether (4:2, 10 mL) **23e**.

*4.2.5.1. 4-(3,4,5-Trimetoxyphenyl)-5-(3-mercapto-4-methoxyphenyl)oxazole (**23c**)*

Yellow crystals. Yield 55% (0.13 g, 0.35 mmol). mp 136-137 °C. R_f (EtOAc/n-hexane, 1:1) 0.35. UV-vis (MeOH) λ_{max} (log ε): 282 (4.31), 240 (4.40). HPLC: 96.38%, tR = 3.23 min. ^{1}H NMR (700 MHz, $CDCl_3$) δ 7.93 (s, 1H, C2ox-**H**), 7.63 (d, J = 2.2 Hz, 1H, C2'-**H**), 7.43 (dd, J = 8.5, 2.1 Hz, 1H, C6'-**H**), 6.95 (s, 2H, C2-**H**, C6-**H**),), 6.89 (d, J = 8.6 Hz, 1H, C5'-**H**), 3.96 (s, 3H, C4-OC**H$_3$**), 3.92 (s, 3H, C4'-OC**H$_3$**), 3.89 (s, 1H, C3'-S**H**), 3.83 (s, 6H, C3-OC**H$_3$**, C5-OC**H$_3$**). ^{13}C NMR (176 MHz, $CDCl_3$) δ 155.14 (**C4'**), 153.36 (**C3**, **C5**), 149.37 (**C2ox**), 144.95 (**C5ox**), 137.98 (**C4**), 133.77 (**C4ox**), 127.68 (**C2'**), 127.42 (**C1**), 125.47 (**C6'**), 121.75 (**C1**'), 121.53 (**C3'**), 110.46 (**C5'**), 104.72 (**C2**, **C6**), 60.98 (C4-O**C**H$_3$), 56.14 (C3-O**C**H$_3$, C5-O**C**H$_3$, 56.09 (C4'-O**C**H$_3$). FTIR ATR (KBr) cm^{-1}: 3134 (νN=C$_{Ar}$-H), 3064 (ν=C$_{Ar}$-H), 2999 (νCH$_3$), 2964 (ν_{as} CH$_3$), 2930 (ν CH$_3$), 2837 (ν O-CH$_3$), 1620 (ν C$_{Ar}$=N), 1583 (ν C$_{Ar}$=C$_{Ar}$), 1512 (ν C$_{Ar}$=C$_{Ar}$), 1451 (δ_{as} CH$_3$), 1374 (δ_s CH$_3$), 1277 (νC-N), 1235 (ν_{as} C$_{Ar}$-O-C), 1121 (νC-O-C), 1069 (ν_s C$_{Ar}$-O-C), 829 (γ^{oop} =C$_{Ar}$-H), 813 (γ^{oop} =C$_{Ar}$-H), 813 (γ^{oop} =C$_{Ar}$-H), 760 (γ^{oop} =C$_{Ar}$-H).

LRMS (EI) m/z 373.0 ([M]$^+$, 100%). HRMS (EI) m/z calcd for $C_{19}H_{19}NO_5S$: 373.0978. Found: 373.0988.

*4.2.5.2. 4-(3,5-Dimethoxy-4-methylthiophenyl)-5-(3-hydroxy-4-methoxyphenyl)oxazole (**23e**)*

Colorless crystals. Yield 62% (0.15 g, 0.39 mmol). mp 160-161 °C. R_f (EtOAc/n-hexane, 1:1) 0.35. UV-vis (MeOH) λ_{max} (log ε): 308 (4.29). HPLC: 98.78%, tR = 2.92 min. ^{1}H NMR (500 MHz, $CDCl_3$) δ 7.92 (s, 1H, C2ox-**H**), 7.26 (s, 1H, C2'-**H**), 7.16 (dd, J = 8.4, 2.2 Hz, 1H, C6'-**H**), 6.94 (s, 2H, C2-**H**, C6-**H**), 6.87 (d, J = 8.3 Hz, 1H, C5'-**H**), 5.70 (s, 1H, C3'-O**H**), 3.93 (s, 3H, C4'-OC**H$_3$**), 3.82 (s, 6H, C3-OC**H$_3$**, C5-OC**H$_3$**), 2.39 (s, 3H, C4-SC**H$_3$**). ^{13}C NMR (126 MHz, $CDCl_3$) δ 160.47 (**C3**, **C5**), 149.34 (**C2ox**), 147.25 (**C4'**), 146.09 (**C5ox**), 145.70 (**C3'**), 133.48 (**C1**), 133.02 (**C4ox**), 121.82 (**C1'**), 119.69 (**C6'**), 113.52 (**C2'**), 111.91 (**C4**), 110.52 (**C5'**), 103.54 (**C2**, **C6**), 56.19 (C3-O**C**H$_3$, C5-O**C**H$_3$), 56.00 (C4'-O**C**H$_3$), 17.84 (C4-S**C**H$_3$). FTIR ATR (KBr) cm^{-1}: 3433 (νO-H), 3120 (νN=C$_{Ar}$-H), 3013 (ν=C$_{Ar}$-H), 2926 (νCH$_3$), 2845 (νO-CH$_3$), 1578 (νC$_{Ar}$=C$_{Ar}$), 1507 (νC$_{Ar}$=C$_{Ar}$), 1463 (δ_{as} CH$_3$), 1374 (δ_s CH$_3$), 1235 (ν_{as} C$_{Ar}$-O-C), 1122 (νC-O-C), 1012 (ν_s C$_{Ar}$-O-C), 846 (γ^{oop} =C$_{Ar}$-H), 809 (γ^{oop} =C$_{Ar}$-H). LRMS (EI) m/z 373.0 ([M]$^+$, 100%). HRMS (EI) m/z calcd for $C_{19}H_{19}NO_5S$: 373.0978. Found: 373.0974.

*4.2.6. General procedure for compounds **24a-b** and **24d-f** (N-methylimidazole-bridged analogues, core 4)*

A mixture of the appropriate benzaldehyde **6a**, **6d**, **8d**, **9d**, and **13** (1 mmol) and 33% $MeNH_2$/EtOH (0.47 g, 5 mmol) in anhydrous ethanol (15 mL) was treated with 0.3 mL of acetic acid and refluxed for 2 h under nitrogen. After the mixture was cooled to room temperature, it was treated with 5 mL of DME, tosylmethyl isocyanides (TosMICs) **20-22** (1.5 mmol), and potassium carbonate (0.55 g, 4 mmol). The reaction mixture was heated at reflux for 3 h. After it was cooled to room temperature, water was added (30 mL) and the mixture was extracted with

ethyl acetate (3x30 mL). The organic layer was separated, washed with brine (100 mL), dried over $MgSO_4$, filtered, and concentrated in vacuo. The residue was purified by flash column chromatography on silica gel ($CHCl_3$/MeOH, 10:1) **24a-b** and **24e-f** or by recrystallization from EtOAc/hexane (1:1) **24d**.

*4.2.6.1. 1-Methyl-4-(3,4,5-trimethoxyphenyl)-5-(2-methylthiophenyl)imidazole (**24a**)*

Pale yellow crystals. Yield 92% (0.34 g, 0.92 mmol). mp 156-158 °C. R_f ($CHCl_3$/MeOH, 10:1) 0.53. UV-vis (MeOH) λ_{max} (log ε): 258 (4.34). HPLC: 100%, tR = 2.16 min. ^{1}H NMR (400 MHz, $CDCl_3$) δ 7.61 (s, 1H, C2im-**H**), 7.49 – 7.41 (m, 1H, C5'-**H**), 7.31 (d, J = 8.1 Hz, 1H, C6'-**H**), 7.25 – 7.23 (m, 2H, C3'-**H**, C4'-**H**), 6.75 (s, 2H, C2-**H**, C6-**H**), 3.78 (s, 3H, N1im-C**H$_3$**), 3.60 (s, 6H, C3-OC**H$_3$**, C5-OC**H$_3$**), 3.42 (s, 3H, C4-OC**H$_3$**), 2.37 (s, 3H, C2'-SC**H$_3$**). ^{13}C NMR (101 MHz, $CDCl_3$) δ 152.87 (**C3**, **C5**), 141.79 (**C2im**), 138.21 (**C4**), 137.22 (**C4'**), 136.33 (**C2'**), 132.04 (**C6'**), 130.01(**C4im**, **C5im**), 128.98 (**C1'**), 126.34 (**C1**), 124.97 (**C5'**), 124.47 (**C3'**), 102.40 (**C2**, **C6**), 60.75 (C4-O**C**H$_3$), 55.52 (C3-O**C**H$_3$, C5-O**C**H$_3$), 31.67 (N1im-**C**H$_3$), 14.82 (C2'-S**C**H$_3$). FTIR ATR (KBr) cm^{-1}: 3098 (νN=C$_{Ar}$-H), 2995 (νCH$_3$), 2954 (ν_{as} CH$_3$), 2934 (ν CH$_3$), 2829 (νO-CH$_3$), 1582 (νC$_{Ar}$=C$_{Ar}$), 1508 (νC$_{Ar}$=C$_{Ar}$), 1415 (δ_{as} CH$_3$), 1330 (δ_s CH$_3$), 1237 (ν_{as} C$_{Ar}$-O-C), 1125 (ν C-O-C), 848 (γ^{oop} =C$_{Ar}$-H), 778 (γ^{oop} =C$_{Ar}$-H). LRMS (EI) m/z 370.2 ([M]$^+$, 100%), 355.2 ([M-CH$_3$]$^+$, 69.1%) HRMS (EI) m/z calcd for $C_{20}H_{22}N_2O_3S$: 370.1346. Found: 370.1339.

*4.2.6.2. 1-Methyl-4-(3,5-dimethoxy-4-methylthiophenyl)-5-(4-methoxy-3-N,N-dimethylthio-carbamoyloxyphenyl)imidazole (**24b**)*

Pale yellow crystals. Yield 51% (0.24 g, 0.51 mmol). mp 192-194 °C. R_f ($CHCl_3$/MeOH, 10:1) 0.45. UV-vis (MeOH) λ_{max} (log ε): 294 (4.28), 246 (4.42). HPLC: 99.30%, tR = 2.26 min. ^{1}H NMR (500 MHz, $CDCl_3$) δ 7.61 (s, 1H, C2im-**H**), 7.20 (dd, J = 8.4, 2.1 Hz, 1H, C6'-**H**), 7.07

(d, *J* = 2.1 Hz, 1H, C2'-**H**), 7.04 (d, *J* = 8.4 Hz, 1H, C5'-**H**), 6.83 (s, 2H, C2-**H**, C6-**H**), 3.87 (s, 3H, N1im-C**H$_3$**), 3.73 (s, 6H, C3-OC**H$_3$**, C5-OC**H$_3$**), 3.52 (s, 3H, C4'-OC**H$_3$**), 3.45 (s, 3H, C8'**H$_3$**), 3.37 (s, 3H, C9'**H$_3$**), 2.33 (s, 3H, C4-SC**H$_3$**). ^{13}C NMR (126 MHz, $CDCl_3$) δ 187.50 (**C7'**), 160.31 (**C3**, **C5**), 152.18 (**C4'**), 143.18 (**C3'**), 137.52 (**C1'**), 137.13 (**C2im**), 129.67 (**C6'**), 128.47 (**C2'**), 126.66 (**C4im**, **C5im**), 122.34 (**C1**), 112.91 (**C5'**), 109.65 (**C4**), 102.32 (**C2**, **C6**), 56.15 (C4'-O**C**H$_3$), 56.07 (C3-O**C**H$_3$, C5-O**C**H$_3$), 43.47 (**C8'**), 38.78 (**C9'**), 32.30 (N1im-**C**H$_3$), 17.92 (C4-S**C**H$_3$). FTIR ATR (KBr) cm^{-1}: 3110 (νN=C$_{Ar}$-H), 3003 (ν=C$_{Ar}$-H), 2957 (ν_{as} CH$_3$), 2933 (νCH$_3$), 2835 (νO-CH$_3$), 1551 (νC$_{Ar}$=C$_{Ar}$), 1510 (νC$_{Ar}$=C$_{Ar}$), 1443 (δ_{as} CH$_3$), 1408 (δ_s CH$_3$), 1270 (νC-N), 1234 (ν_{as} C$_{Ar}$-O-C), 1110 (νC-O-C), 1024 (ν_s C$_{Ar}$-O-C), 846 (γ^{oop} =C$_{Ar}$-H), 817 (γ^{oop} =C$_{Ar}$-H). LRMS (EI) m/z 473.3 ([M]$^+$, 100%), 88.0 ([(CH$_3$)NCS]$^+$, 77.6%). HRMS (EI) m/z calcd for $C_{23}H_{27}N_3O_4S_2$: 473.1437. Found: 473,1442.

*4.2.6.3. 1-Methyl-4-(3,4,5-trimethoxyphenyl)-5-(3-bromo-5-methoxy-4-methylthiophenyl)-imidazole (**24d**)*

White crystals. Yield 29% (0.14 g, 0.29 mmol). mp 126-130 °C. R_f ($CHCl_3$/MeOH, 10:1) 0.53. UV-vis (MeOH) λ_{max} (log ε): 282 (4.11). HPLC: 97.44%, tR = 2.54 min. ^{1}H NMR (500 MHz, $CDCl_3$) δ 7.56 (s, 1H, C2im-**H**), 7.33 (d, *J* = 1.2 Hz, 1H, C2'-**H**), 6.80 (d, *J* = 1.3 Hz, 1H, C6'-**H**), 6.77 (s, 2H, C2-**H**, C6-**H**), 3.82 (s, 3H, N1im-C**H$_3$**), 3.81 (s, 3H, C5'-OC**H$_3$**), 3.67 (s, 6H, C3-OC**H$_3$**, C5-OC**H$_3$**), 3.55 (s, 3H, C4-OC**H$_3$**), 2.43 (s, 3H, C4'-SC**H$_3$**). ^{13}C NMR (126 MHz, $CDCl_3$) δ 160.94 (**C5'**), 152.99 (**C3**, **C5**), 138.64 (**C4**), 137.64 (**C2im**), 136.85 (**C3'**), 132.55 (**C4im**), 130.55 (**C5im**), 129.60 (**C4'**), 127.15 (**C1**), 126.66 (**C2'**), 126.65 (**C1'**), 112.54 (**C6'**), 103.49 (**C2**, **C6**), 60.87 (C4-O**C**H$_3$), 56.52 (C5'-O**C**H$_3$), 55.74 (C3-O**C**H$_3$, C5-O**C**H$_3$), 32.35 (N1im-**C**H$_3$), 18.16 (C4'-S**C**H$_3$). FTIR ATR (KBr) cm^{-1}: 3101 (νN=C$_{Ar}$-H), 3065 (ν=C$_{Ar}$-H), 2963 (ν_{as} CH$_3$), 2924 (νCH$_3$), 2829 (νO-CH$_3$), 1584 (νC$_{Ar}$=C$_{Ar}$), 1510 (νC$_{Ar}$=C$_{Ar}$), 1463

(δ_{as} CH_3), 1397 (δ_s CH_3), 1235 (ν_{as} C_{Ar}-O-C), 1125 (νC-O-C), 1028 (ν_s C_{Ar}-O-C), 839 (γ^{oop} =C_{Ar}-H), 780 (γ^{oop} =C_{Ar}-H). LRMS (EI) m/z 480.1 ([M^+ + 2], 58.6%), 478,0 ([M]$^+$, 55.8%), 465.1 ([M^+ + 2 - CH_3], 45.1%), 463.0 ([M-CH_3]$^+$, 43.7%), 414.1 (100%), 399.1 ([M-Br]$^+$, 73.4%). HRMS (EI) m/z calcd for $C_{21}H_{23}BrN_2O_4S$: 478.0556. Found: 478.0560.

*4.2.6.4. 1-Methyl-4-(3-bromo-4,5-dimethoxyphenyl)-5-(3-methoxy-4-methylthiophenyl)-imidazole **(24e)***

Yellow crystals. Yield 27% (0.12 g, 0.27 mmol). mp 130-135 °C. R_f ($CHCl_3$/MeOH, 10:1) 0.61. UV-vis (MeOH) λ_{max} (log ε): 260 (5.53). HPLC: 99.29%, tR = 2.48 min. ^{1}H NMR (500 MHz, $CDCl_3$) δ 7.54 (s, 1H, C2im-**H**), 7.33 (d, J = 2.0 Hz, 1H, C2-**H**), 7.23 (d, J = 7.9 Hz, 1H, C5'-**H**), 7.04 (d, J = 1.9 Hz, 1H, C6-**H**), 6.95 (dd, J = 7.9, 1.7 Hz, 1H, C6'-**H**), 6.76 (d, J = 1.6 Hz, 1H, C2'-**H**), 3.84 (s, 3H, N1im-C**H$_3$**), 3.80 (s, 3H, C5-OC**H$_3$**), 3.64 (s, 3H, C4-OC**H$_3$**), 3.49 (s, 3H, C3'-OC**H$_3$**), 2.48 (s, 3H, C4'-SC**H$_3$**). ^{13}C NMR (126 MHz, CDCl3) δ 156.31 (**C3'**), 153.15 (**C5**), 144.79 (**C4**), 137.34 (**C2im**), 136.53 (**C4im**), 131.75 (**C5im**), 128.74 (**C1'**), 128.69 (**C1**), 127.28 (**C4'**), 125.78 (**C2**), 123.37 (**C5'**), 122.41 (**C6'**), 117.40 (**C3**), 111.97 (**C6**), 109.80 (**C2'**), 60.54 (C4-O**C**H_3), 56.04 (C3'-O**C**H_3), 55.69 (C5-O**C**H_3), 32.19 (N1im-**C**H_3), 14.42 (C4'-S**C**H_3). FTIR ATR (KBr) cm^{-1}: 3101 (ν N=C_{Ar}-H), 2933 (ν CH_3), 2829 (ν O-CH_3), 1557 (ν C_{Ar}=C_{Ar}), 1506 (ν C_{Ar}=C_{Ar}), 1463 (δ_{as} CH_3), 1402 (δ_s CH_3), 1231 (ν_{as} C_{Ar}-O-C), 1043 (ν_s C_{Ar}-O-C), 853 (γ^{oop} =C_{Ar}-H). LRMS (EI) m/z 450.1 ([M^+ + 2], 100%), 448.0 ([M]$^+$, 94.7%), 435.1 ([M^+ + 2 - CH_3], 42.5%), 433.0 ([M-CH_3]$^+$, 40.7%). HRMS (EI) m/z calcd for $C_{20}H_{21}BrN_2O_3S$: 448.0451. Found: 448,0458.

*4.2.6.5. 1-Methyl-4-(3-bromo-4,5-dimethoxyphenyl)-5-(4-methoxy-3-methylthiophenyl)-imidazole **(24f)***

Yellow crystals. Yield 38% (0.17 g, 0.38 mmol). mp 130-135 °C. R_f ($CHCl_3$/MeOH, 10:1) 0.69. UV-vis (MeOH) λ_{max} (log ε): 259 (5.45). HPLC: 96.24%, tR = 2.41 min. ^{1}H NMR (500

MHz, $CDCl_3$) δ 7.54 (s, 1H, C2im-**H**), 7.32 (d, J = 1.6 Hz, 1H, C2'-**H**), 7.11 (dd, J = 6.5, 1.7 Hz, 1H, C6'-**H**), 7.09 (d, J = 1.6 Hz, 1H, C2-**H**), 7.05 (d, J = 1.6 Hz, 1H, C6-**H**), 6.93 (d, J = 6.5 Hz, 1H, C5'-**H**), 3.96 (s, 3H, N1im-C**H$_3$**), 3.80 (s, 3H, C5-OC**H$_3$**), 3.65 (s, 3H, C4-OC**H$_3$**), 3.48 (s, 3H, C4'-OC**H$_3$**), 2.36 (s, 3H, C3'-SC**H$_3$**). ^{13}C NMR (126 MHz, $CDCl_3$) δ 156.55 (**C5**), 153.17 (**C4'**), 144.76 (**C4**), 137.22 (**C2im**), 136.53 (**C4im**), 131.87 (**C5im**), 128.71 (**C1'**), 128.38 (**C1**), 128.14 (**C2'**), 127.86 (**C2**), 122.90 (**C3'**), 122.37 (**C6'**), 117.43 (**C3**), 110.28 (**C5'**), 109.70 (**C6**), 60.56 (C4-O**C**H_3), 56.01 (C4'-O**C**H_3), 55.71 (C5-O**C**H_3), 32.16 (N1im-**C**H_3), 14.70 (C3'-S**C**H_3). FTIR ATR (KBr) cm^{-1}: 3097 (ν N=C_{Ar}-H), 3005 (ν =C_{Ar}-H), 2930 (ν CH_3), 2832 (ν O-CH_3), 1562 (νC_{Ar}=C_{Ar}), 1523 (νC_{Ar}=C_{Ar}), 1437 (δ_{as} CH_3), 1382 (δ_s CH_3), 1249 (ν_{as} C_{Ar}-O-C), 1044 (ν_s C_{Ar}-O-C), 877 (γ^{oop} =C_{Ar}-H). LRMS (EI) m/z 450.1 ([M^+ + 2], 100%), 448.0 ([M]$^+$, 96.4%), 435.1 ([M^+ + 2 - CH_3], 44.3%), 433.0 ([M-CH_3]$^+$, 43.3%). HRMS (EI) m/z calcd for $C_{20}H_{21}BrN_2O_3S$: 448.0451. Found: 448.0457.

*4.2.7. Procedure for the synthesis of compound **24c** (N-methylimidazole-bridged analogue, core 4)*

A mixture of **24b** (0.14 g, 0.3 mmol) and 10% KOH/MeOH (3 mL) was heated at 80 °C under nitrogen for 5.5 h. Upon cooling the mixture was acidified with acetic acid to pH 4-5. The precipitated crude product was collected by filtration, washed with water, and purified by recrystallization from isopropanol (5 mL) with the use of activated carbon to afford pure product **24c** as white crystals.

*4.2.7.1. 1-Methyl-4-(3,5-dimethoxy-4-methylthiophenyl)-5-(3-hydroxy-4-methoxyphenyl)-imidazole (**24c**)*

White crystals. Yield 33% (39 mg, 0.10 mmol). mp 123-125 °C. R_f ($CHCl_3$/MeOH, 10:1) 0.38. UV-vis (MeOH) λ_{max} (log ε): 292 (4.52). HPLC: 100%, tR = 1.86 min. ^{1}H NMR (500 MHz, $CDCl_3$) δ 7.61 (s, 1H, C2im-**H**), 6.97 – 6.92 (m, 2H, C2'-**H**, C6'-**H**), 6.85 (dd, J = 8.2, 2.1

Hz, 1H, C5'-**H**), 6.81 (s, 2H, C2-**H**, C6-**H**), 5.87 (s, 1H, C3'-O**H**), 3.95 (s, 3H, N1im-C**H$_3$**), 3.69 (s, 6H, C3-OC**H$_3$**, C5-OC**H$_3$**), 3.49 (s, 3H, C4'-OC**H$_3$**), 2.32 (s, 3H, C4-SC**H$_3$**). ^{13}C NMR (126 MHz, $CDCl_3$) δ 160.26 (**C3**, **C5**), 147.23 (**C4'**), 147.12 (**C3'**), 146.13 (**C2im**), 137.18 (**C4im**), 136.82 (**C1'**), 129.25 (**C1**), 123.27 (**C5im**), 123.00 (**C6'**), 116.78 (**C2'**), 111.03 (**C5'**), 109.65 (**C4**), 102.20 (**C2**, **C6**), 56.10 (C4'-O**C**H_3), 55.87 (C3-O**C**H_3, C5-O**C**H_3), 32.19 (N1im-**C**H_3), 17.92 (C4-S**C**H_3). FTIR ATR (KBr) cm^{-1}: 3433 (ν O-H), 3119 (ν N=C_{Ar}-H), 2950 (ν_{as} CH_3), 2935 (ν CH_3), 2836 (ν O-CH_3), 1596 (ν C_{Ar}=C_{Ar}), 1513 (ν C_{Ar}=C_{Ar}), 1452 (δ_{as} CH_3), 1363 (δ_s CH_3), 1252 (ν C-N), 1241 (ν_{as} C_{Ar}-O-C), 1114 (ν C-O-C), 1023 (ν_s C_{Ar}-O-C), 838 (γ^{oop} =C_{Ar}-H), 815 (γ^{oop} =C_{Ar}-H). LRMS (EI) m/z 386.2 ($[M]^+$, 100%). HRMS (EI) m/z calcd for $C_{20}H_{22}N_2O_4S$: 386.1295. Found: 386.1304.

4.3 Molecular modeling

4.3.1 Generation of the virtual combinatorial library (VCL)

Based on the elaborated synthetic protocol for CA-4 analogues (Scheme 2-6), two sets of queries were defined. The first (BB1 query) described molecular pattern was for differently substituted aromatic aldehydes and the second for phenylacetic acids (BB2 query). The in-house building blocks (and intermediates) library was screened using a substructure searching the algorithm and defined automatic queries by means of tools available in the JChem library (detailed results are presented in Supporting Information). Selected building blocks BB1 (48 compounds) and BB2 (7 compounds) were then iteratively combined with four cores (α-phenylcinnamic acids – core 1; (*Z*)-stilbenes – core 2; 4,5-disubstituted oxazoles – core 3, and 4,5-disubstituted N-methylimidazoles – core 4) using CombiGlide [65]. This way all possible combinations (1,159 structures), i.e. virtual compounds, were produced and used as an input database for the parallel virtual screening protocol.

4.3.1 Parallel virtual screening protocol

Each VCL compound was simultaneously evaluated by means of the developed screening protocol including 3-dimensional pharmacophore, QSAR models, and the post-docking scoring method. The models were trained and tested using a set of actives and decoys (generated based on DUD methodology) [66]. For each model a threshold (classification cut-off) was obtained based on the ROC curve. Detailed results of the models evaluation are in Supporting Information.

4.3.2 3-Dimensional pharmacophore filter

The 3-dimensional pharmacophore model was obtained by using the 3D QSAR Pharmacophore Generation protocol implemented in Discovery Studio 3.5. The structures of 21 compounds, fetched from ref. [67], were used as a training set. The conformation space of each reference compound was generated using the BEST algorithm within a relative energy threshold of 20 kcal/mol above the global energy minimum and with a maximum number of generated conformations per ligand set to 255. Four types of features were used to define the pharmacophore hypotheses, i.e. the hydrogen bond acceptor (HBA), hydrogen bond donor (HBD), hydrophobic feature (HYD), and hydrophobic aromatic group (HY-AR), but maximum features used to build the model were set to 5. The minimum distance between features was fixed at 2.5 Å. In this study, the top 10 pharmacophore hypotheses were returned by the generation process and further used in the evaluation calculations.

4.3.3 QSAR filter

Two QSAR models (Bayesian and Multiple Linear Regression) were generated using Discovery Studio 3.5. In order to train and test the generated models, a total of 48 and 35 compounds with experimental activity data were selected from reported articles [18,68],

respectively. Bayesian QSAR models were generated by means of the Create Bayesian Model protocol. The training set was divided into two categories, i.e. active (class 1) and inactive (class 0, for details, see Supporting Information), using different cut-offs for IC_{50}. The following set of 2D descriptors was used in model building: extended connectivity fingerprints with a maximum diameter of 6 (ECFP_6), AlogP, molecular weight, number of rotatable bonds, number of rings, number of aromatic rings, number of hydrogen bond acceptors, number of hydrogen bond donors, and molecular fractional polar surface. The models were validated using leave-one-out, cross-validation, and external test set methods. The Best Split value was calculated by picking the split that minimized the sum of the percentage misclassified for category inhibitors and for category non-inhibitors by using the cross-validated score for each sample. Using that split, a contingency table was constructed containing the number of true positives (TP), false negatives (FN), false positives (FP), and true negatives (TN). Sensitivity (SE), specificity (SP), and overall prediction accuracy (Q) were also calculated and compared to select the best model (see Supporting Information).

The Multiple Linear Regression QSAR model was generated using the same sets of training, testing, and 2D molecular descriptors as were used in the creation of the Bayesian QSAR model.

4.3.4 Docking filter

The two crystal structures of tubulin in complex with colchicine (PDB ID: 1SA0) and podophyllotoxin (PDB ID: 1SA1) as published by Ravelli et al. [69] were retrieved from the Protein Data Bank (http://www.rcsb.org/pdb/home/home.do). 3-Dimensional structures of all the compounds from VCL were prepared using LigPrep [70] and the appropriate ionization states at pH = 7.4 were assigned using Epik [71]. The Protein Preparation Wizard was used to assign bond orders, check the steric clashes, and assign appropriate amino acid ionization states. The

receptor grids were generated (the OPLS_2005 force field) by setting the grid box on the center of the co-crystalized ligand. Automated docking was performed by using Glide at SP level with the flexible docking option turned on [72]. The docking procedure was validated by re-docking of co-crystallized ligands (i.e. CN2 and POD for 1SA0 and 1SA1, respectively) to the tubulin active site, which resulted in the predicted docking pose with RMSD lower than 1 Å, calculated for the best scored pose. Each 3-dimensional ligand-protein complex was then encoded using an in-house implementation of Structural Interaction Fingerprints (SIFt). The results were stored in the form of a 1D binary string, where a nine-bit pattern was used to describe the interaction type, i.e. any contact, backbone, side chain, polar, aromatic, hydrophobic interaction, hydrogen bond donor/acceptor, and charged [73]. Tanimoto metric and SIFt vectors were used to calculate similarity between the co-crystallized ligand and the docked VCL compounds.

4.3.5 Ranking scheme

The final ranking list of VCL compounds was made by merging rankings obtained by each filter, such as Tanimoto coefficients calculated for 1SA0 and 1SA1, Fit Value produced by mapping ligands to the pharmacophore model, and QSAR model predictions. For each of the parameters, separate rankings were created and merged into one using the SUM rule of data fusion [74].

4.3.6 External validation test set

The external validation test set was composed of 20 tubulin inhibitors and 800 decoys. Compounds having IC_{50} < 100 nM of tubulin inhibition were fetched from the ChEMBL v. 16 database. Then structures used in training (21 and 48 for pharmacophore generation and QSAR models, respectively) and testing (35) of the VCL models were removed using a substructure searching algorithm implemented in Instant JChem [75]. The remaining set was hierarchically

grouped using the Molprint2D fingerprint and Tanimoto metric (Canvas) [76], yielding 20 clusters. Due to different cluster size, only centroids were selected as an active part of the test set. The decoy set was generated based on DUD methodology using DUD-e service [66].

4.4 Biological evaluation

4.4.1 Materials for biological activity in vitro

Dulbecco's Modified Eagle's Medium (DMEM) without phenol red, heat-inactivated fetal bovine serum (FBS), 0.25% trypsin-EDTA solution, phosphate buffered saline (PBS), 3-(4,5-dimethylthiazol-2-yl)-2,5-diphenyltetrazolium bromide (MTT), dimethyl sulfoxide, propidium iodide, Hoechst 33258, Monoclonal Anti-α-Tubulin−FITC antibody, paraformaldehyde, bovine serum albumin, Triton X-100, and RNAse A were obtained from Sigma-Aldrich (St. Louis, Mi, USA). Dimethyl sulfoxide was obtained from Avantor (Gliwice, Poland) and penicillin-streptomycin and L-glutamine solutions were obtained from Life Technologies (Grand Island, NY, USA). Cell Death Detection ELISA^{PLUS} kits were obtained from Roche (Basel, Switzerland). All cell culture consumables were purchased from BD Falcon (Franklin Lakes, NJ, USA).

4.4.2 Cell culture

Several human cancer cell lines were used to determine the cytotoxicity of the tested compounds. These cancer cell lines were: A431 (human epidermoid carcinoma), A549 (human lung adenocarcinoma), CCD39Lu (normal human lung fibroblast), HaCaT (human immortalized non-cancerous keratinocyte), HeLa (human cervical adenocarcinoma), MCF-7 (human breast adenocarcinoma), MDA-MB-231 (human breast adenocarcinoma), and SKOV-3 (human ovarian adenocarcinoma). All cell lines were obtained from the European Collection of Cell Cultures

(ECACC, Salisbury, UK) and cultured in DMEM supplemented with 10% FBS, penicillin (100 U/mL), streptomycin (0.1 mg/mL), and L-glutamine (2 mM).

4.4.3 Tested compounds

Stock solutions (10 mM) of the following tested compounds **14a-b**, **15a-b**, **23a**, **23c**, **23e-j**, **24a**, **24c-f**, and CA-4 were prepared by dissolving in DMSO and storing them at -20 ºC.

4.4.4 Cell viability assay

The cytotoxicity of the tested compounds was determined using the MTT assay. The MTT is a water-soluble dye which can be reduced to water-insoluble purple formazan crystals by mitochondrial dehydrogenase only in metabolically active cells [77].

Cells were seeded at a density of 2×10^4 cells per well in 96-well plates and incubated overnight under cell culture conditions. The tested compounds were added at concentrations of 0.6 μM, 1.2 μM, 2.5 μM, 5 μM, 10 μM, and 20 μM and incubated for 48 h. After incubation the medium was aspirated and the freshly prepared solution (170 μL) containing the MTT solution (5 mg/mL PBS) in culture medium was added to each well. The cells were incubated 2 h under cell culture conditions, then centrifuged for 3 min and formazan crystals were dissolved in 200 μL DMSO. Absorbance was measured at 570 nm with a plate reader (Biotek Instruments, Elx-800). Cell viability was calculated as a percentage of the control. The results are presented as the mean ± SD from three independent experiments.

4.4.5 In vitro tubulin polymerization assay

The effect of the synthesized compounds **14a-b**, **15a-b**, **23a**, **23c**, **23e-j**, **24a**, **24c-f**, and CA-4 on tubulin polymerization *in vitro* was studied with the use of purified porcine tubulin purchased from Cytoskeleton Inc. Denver, CO, USA (Cat. # BK004P) according to a protocol

recommended by the manufacturer. Tubulin was dissolved in buffer containing 80 mM PIPES pH 6.9, 2 mM $MgCl_2$, 0.5 mM EGTA, and 1 mM GTP at a final concentration of 3 mg/mL and pipetted into a 96-well plate (0.3 mg per well). The polymerization reaction was started by increasing the temperature from 4 ºC to 37 ºC upon transfer of the reaction mixture to a pre-warmed plate. The assembly of microtubules was monitored spectrophotometrically by following the change of absorbance at 350 nm over time (60 min). The spectrophotometer was temperature-regulated and set at 37 ºC. Under standard conditions, polymerization control (with the vehicle only) achieved a maximal OD340 between 0.15 – 0.25 within 30 min at 37 ºC; CA-4 was used as a positive control. V_{max} of tubulin polymerization was determined. The concetration that inhibited tubulin polymerization by 50% (IC_{50}) was calculated using GraphPad Prism software version 5.00 (GraphPad Inc., La Jolla, CA, USA).

4.4.6 Cell cycle analysis

Propidium iodide staining was performed to analyze cell cycle redistribution in response to treatment with **23e**, **23i**, and CA-4. Briefly, A431, HaCaT, HeLa, MCF-7, MDA-MB-231, and SKOV-3 cells were seeded at a density of 5×10^5 cells per well and incubated overnight under cell culture conditions. Then the cells were treated with **23e**, **23i**, and CA-4 at the following concentrations: 0.1 μM, 0.5 μM, and 1 μM for 24 h. DMSO was used as a negative control. Then the cells were harvested by trypsinization, centrifuged at 5000 rpm, and washed twice with PBS. The samples were fixed for 30 min in 70% ethanol at 4 ºC, centrifuged again, and washed two times with PBS. The cells were stained with 50 μg/mL of propidium iodide in the presence of 100 μg/mL RNAse A (Sigma-Aldrich, St. Louis, MO, USA) for 30 min in dark conditions. Then the samples were analyzed using a fluorescence-activated cell sorter (FACS) Calibur

(Becton&Dickinson, USA). The results are presented as the mean ± SD from three independent experiments.

4.4.7 Apoptosis assay

Apoptosis was evaluated using a commercially available kit (Cell Death Detection ELISA^{PLUS}, Roche) according to manufacturer's protocol. The kit allows to quantify mono- and oligonucleosomes formed in apoptotic cells [78].

MCF-7, MDA-MB-231, HeLa, SKOV3, HaCaT, and A431 cells (2×10^4) were incubated with compounds **23e**, **23i**, and CA-4 at concentrations of 0.1 μM, 0.5 μM, and 1 μM. After 24 h of incubation the cells were lysed and the supernatant was collected after centrifugation at 1200 rpm for 10 min. The lysates were transferred to a streptavidin-coated plate and incubated for 2 h with a reaction mixture containing anti-histone-biotin, anti-DNA-peroxidase, and buffer. After the washing step, ABTS [2,2'-azinobis-(3-ethylbenzthiazoline-6-sulfonic acid)] was added and they were incubated for 30 min. Then the plates were washed and absorbance at 405 nm was measured using a plate reader (Biotek Instruments, Elx-800). The results are presented according to the manufacturer's suggestion as an enrichment factor (EF) and are shown as the means ± SD from three independent experiments.

4.4.8 Apoptosis assessment: annexin V and propidium iodide labeling

Annexin V detection was performed using FITC Annexin V Apoptosis Detection Kit I (BD Biosciences, USA) according to the manufacturer's protocol. Briefly, after being treated with the test compounds **23e**, **23i**, and CA-4 for 24 h the cells were then transferred (100 μl of the solution (1×10^6 cells) to a 5 mL culture tube followed by application of 5 μl Annexin-V-Fluos and 5 μl propidium iodide. The samples were gently mixed and incubated for 15 min at RT (25 ºC) in the dark. Finally, the samples were analyzed by a FACScan Flow Cytometer (Becton

Dickinson, USA). Laser excitation wavelength was set at 488 nm. The green signal from annexin V-FITC was measured at 525 nm and the red signal from PI was measured at 620 nm.

4.4.9 Immunochemistry experiments

MCF-7, MDA-MB-231, HeLa, SKOV3, HaCaT, and A431 cells were seeded at a density of $12.5x10^4$ cells per well in 24-well plates. The cells were treated with **23e**, **23i**, and CA-4 at a concentration of 1 μM for 24 h. The cells were incubated with Hoechst 33258 at a concentration of 10 μg/mL for 30 min at 37 ºC. Then the cells were washed twice with PBS and fixed with 4% formaldehyde in phosphate buffer saline (PBS) for 15 min at room temperature and washed twice with PBS. The cells were permeabilized with 1% Triton X-100 and incubated with a blocking solution (2% BSA in PBS) for 1 h at room temperature. Subsequently, anti-α-tubulin-FITC (1:50) antibodies were added and incubated overnight at 4 ºC. Images were captured using a Nikon Eclipse TS100 fluorescence microscope with an attached fluorescence unit model (C-SHG) and a DS-SMc digital camera.

4.4.10 Statistical analysis

Statistical analysis was performed with one-way analysis of variance ANOVA followed by Dunnett's multiple comparison test using GraphPad Prism software version 5.00 (GraphPad Inc., La Jolla, CA, USA). The results are presented as the means ± SD from at least three independent experiments or confidence intervals are used for inhibiton of tubulin polymerization. Unless otherwise indicated, the differences were considered to be statistically significant at $P < 0.05$.

Appendix. Supplementary data

Synthesis and characterization of bromobenzaldehydes (**9**, **10)**. Synthesis and characterization of O-aryl thiocarbamates (**6a**, **8a-9a**, **11a-12a**), S-aryl thiocarbamates (**6b**, **8b-9b**, **11b-12b**), 3-

dioxolane derivatives of S-aryl thiocarbamates (**9c**, **12c**), methylthiobenzaldehydes (**6d**, **8d-9d**, **11d-12d**), tosylmethyl formamides (**17-19**), and tosylmethyl isocyanides – TosMICs (**20-22**) as well as their NMR spectra. NMR spectra and HPLC chromatograms for **7**, **CA-4**, **23b**, **23d**, and **24b** and target compounds **14a-b**, **15a-b**, **23a**, **23c**, **23e-j**, **24a**, and **24c-f**; additional detailed results of the models' evaluation in the virtual screening protocol such as 3-dimensional pharmacophore models, docking filter, and QSAR models.

Acknowledgments

This work was supported by the National Science Centre through grant no. DEC-2011/03/B/NZ7/00509.

Abbreviations used

CA-4, combretastatin A-4; MIAs, microtubule-interfering agents; MDR, multidrug resistance; VDA, vascular-disrupting agent; SAR, structure-activity relationship; VCL, virtual combinatorial library; VS, virtual screening; TosMICs, tosylmethyl isocyanides; LRMS, low-resolution mass spectrometry; HRMS, high-resolution mass spectrometry; SIFt, structural interaction fingerprints; DMEM, Dulbecco's Modified Eagle's Medium; FBS, fetal bovine serum; PBS, phosphate buffered saline; MTT, 3-(4,5-dimethylthiazol-2-yl)-2,5-diphenyltetrazolium bromide; EGTA, ethylene glycol bis(*β*-aminoethyl ether)-N,N,N',N'-tetraacetic acid; GTP, guanosine triphosphate; ABTS, [2,2'-azinobis-(3-ethylbenzthiazoline-6-sulfonic acid)].

References

[1] A. Desai, T.J. Mitchison, Microtubule polymerization dynamics, Annu. Rev. Cell Dev. Biol. 13 (1997) 83–117.

[2] E. Nogales, S.G. Wolf, K.H. Downing, Structure of the alpha beta tubulin dimer by electron crystallography, Nature 391 (1998) 199–203.

[3] K.H. Downing, E. Nogales, Tubulin structure : insights into microtubule properties and functions, Curr. Opin. Struct. Biol. 8 (1998) 785–791.

[4] S.L. Kline-Smith, C.E. Walczak, Mitotic spindle assembly and chromosome segregation: refocusing on microtubule dynamics, Mol. Cell. 15 (2004) 317–327.

[5] P.M. Checchi, J.H. Nettles, J. Zhou, J.P. Snyder, H.C. Joshi, Microtubule-interacting drugs for cancer treatment, Trends Pharmacol. Sci. 24 (2003) 361–365.

[6] M.A. Jordan, L. Wilson, Microtubules as a target for anticancer drugs, Nat. Rev. Cancer. 4 (2004) 253–265.

[7] S. Honore, E. Pasquier, D. Braguer, Understanding microtubule dynamics for improved cancer therapy, Cell. Mol. Life Sci. 62 (2005) 3039–3056.

[8] D.G.I. Kingston, Tubulin-interactive natural products as anticancer agents, J. Nat. Prod. 72 (2009) 507–515.

[9] R.A. Stanton, K.M. Gernert, J.H. Nettles, R. Aneja, Drugs that target dynamic microtubules: a new molecular perspective, Med. Res. Rev. 31 (2011) 443–481.

[10] R. Mikstacka, T. Stefański, J. Różański, Tubulin-interactive stilbene derivatives as anticancer agents, Cell. Mol. Biol. Lett. 18 (2013) 368–97.

[11] R. Kaur, G. Kaur, R. Kaur, R.K. Gill, R. Soni, J. Bariwal, Recent developments in tubulin polymerization inhibitors : An overview, Eur. J. Med. Chem. 87 (2014) 89–124.

[12] M. Abal, J.M. Andreu, I. Barasoain, Taxanes: microtubule and centrosome targets, and cell cycle dependent mechanisms of action, Curr. Cancer Drug Targets 3 (2003) 193–203.

[13] R.M. Buey, I. Barasoain, E. Jackson, A. Meyer, P. Giannakakou, I. Paterson, S. Mooberry, J.M. Andreu, J.F. Díaz, Microtubule interactions with chemically diverse stabilizing agents: thermodynamics of binding to the paclitaxel site predicts cytotoxicity, Chem. Biol. 12 (2005) 1269–1279.

[14] G.M. Cragg, D.G.I. Kingston, D.J. Newman, Anticancer agents from natural products, The vinca alkaloids, 2nd ed.; F. Roussi, F. Guéritte, J. Fahy, CRC Press (2012) pp 177-198.

[15] B. Gigant, C. Wang, R.B.G. Ravelli, F. Roussi, M.O. Steinmetz, P.A. Curmi, A. Sobel, M. Knossow, Structural basis for the regulation of tubulin by vinblastine, Nature 435 (2005) 519–522.

[16] D.L. Sackett, Podophyllotoxin, steganacin and combretastatin: natural products that bind at the colchicine site of tubulin, Pharmac. Ther. 59 (1993) 163–228.

[17] R.M. Lee, D.A. Gewirtz, Colchicine site inhibitors of microtubule integrity as vascular disrupting agents, Drug Dev. Res. 69 (2008) 352–358.

[18] Y. Lu, J. Chen, M. Xiao, W. Li, D.D. Miller, An overview of tubulin inhibitors that interact with the colchicine binding site, Pharm. Res. 29 (2012) 2943–2971.

[19] Y.M. Liu, H.L. Chen, H.Y. Lee, J.P. Liou, Tubulin inhibitors: a patent review, Expert Opin. Ther. Pat. 24 (2014) 69–88.

[20] G.M. Cragg, D.G.I. Kingston, D.J. Newman, Anticancer agents from natural products.

The discovery and development of the combretastatins, 2nd ed.; K.G. Pinney,G.R. Pettit, M.L. Trawick, C. Jelinek, D.J. Chaplin, CRC Press (2012) pp 27-64.

[21] G.R. Pettit, G.M. Cragg, D.L. Herald, J.M. Schmidt, P. Lohavanijaya, Isolation and structure of combretastatin, Can. J. Chem. 60 (1982) 1374–1376.

[22] G.R. Pettit, S.B. Singh, M.L. Niven, E. Hamel, J.M. Schmidt, Isolation, structure, and synthesis of combretastatins A-1 and B-1, potent new inhibitors of microtubule assembly, derived from combretum caffrum, J. Nat. Prod. 50 (1987) 119–131.

[23] G.R. Pettit, S.B. Singh, Isolation, structure, and synthesis of combretastatin A-2, A-3, and B-2, Can. J. Chem. 65 (1987) 2390–2396.

[24] G.R. Pettit, S.B. Singh, M.R. Boyd, E. Hamel, R.K. Pettit, J.M. Schmidt, F. Hogan, Antineoplastic agents. 291. Isolation and synthesis of combretastatins A-4, A-5, and A-6, J. Med. Chem. 38 (1995) 1666-1672.

[25] G.R. Pettit, S.B. Singh, E. Hamel, C.M. Lin, D.S. Alberts, D. Garcia-Kendal, Isolation and structure of the strong cell growth and tubulin inhibitor combretastatin A-4, Experientia. 45 (1989) 209–211.

[26] J. Griggs, J.C. Metcalfe, R. Hesketh, Targeting tumour vasculature: the development of combretastatin A4, Lancet Oncol. 2 (2001) 82–87.

[27] G.M. Tozer, C. Kanthou, C.S. Parkins, S.A. Hill, The biology of the combretastatins as tumour vascular targeting agents, Int. J. Exp. Pathol. 83 (2002) 21–38.

[28] P.E. Thorpe, Vascular targeting agents as cancer therapeutics, Clin. Cancer Res. 10 (2004) 415–427.

[29] A. Chaudhary, S.N. Pandeya, P. Kumar, P.P. Sharma, S. Gupta, N. Soni, K.K. Verma, G. Bhardwaj, Combretastatin A-4 analogs as anticancer agents, Mini-Rev. Med. Chem. 7 (2007) 1186–1205.

[30] L.M. Greene, M.J. Meegan, D.M. Zisterer, Combretastatins : more than just vascular targeting agents ?, J. Pharmacol Exp. Ther. 355 (2015) 212–227.

[31] K. Jaroch, M. Karolak, P. Gorski, A. Jaroch, A. Krajewski, A. Ilnicka, A. Sloderbach, T. Stefanski, S. Sobiak, Combretastatins : in vitro structure-activity relationship, mode of action and current clinical status, Pharmacol. Reports 68 (2016) 1266–1275.

[32] M. Cushman, D. Nagarathnam, D. Gopal, H.M. He, C.M. Lin, E. Hamel, Synthesis and evaluation of analogs of (Z)-1-(4-methoxyphenyl)-2-(3,4,5-trimethoxyphenyl) ethene as potential cytotoxic and antimitotic agents, J. Med. Chem. 35 (1992) 2293–2306.

[33] T. Hatanaka, K. Fujita, K. Ohsumi, R. Nakagawa, Y. Fukuda, Y. Nihei, Y. Suga, Y. Akiyama, T. Tsuji, Novel B-ring modified combretastatin analogues: syntheses and antineoplastic activity, Bioorg. Med. Chem. Lett. 8 (1998) 3371–3374.

[34] K. Gaukroger, J.A. Hadfield, L.A. Hepworth, N.J. Lawrence, A.T. McGown, Novel syntheses of cis and trans isomers of combretastatin A-4, J. Org. Chem. 66 (2001) 8135–8138.

[35] H.N. Nguyen, Combretastatin A-4 analogues as antimitotic antitumor agents., Curr. Med. Chem. 10 (2003) 1697–722.

[36] G.C. Tron, T. Pirali, G. Sorba, F. Pagliai, S. Busacca, A.A. Genazzani, Medicinal chemistry of combretastatin A4: present and future directions, J. Med. Chem. 49 (2006)

3033–3044.

[37] M.S. Gerova, S.R. Stateva, E.M. Radonova, R.B. Kalenderska, R.I. Rusew, R.P. Nikolova, C.D. Chanev, B.L. Shivachev, M.D. Apostolova, O.I. Petrov, Combretastatin A-4 analogues with benzoxazolone scaffold: Synthesis, structure and biological activity, Eur. J. Med. Chem. 120 (2016) 121–133.

[38] L.M. Lima, E.J. Barreiro, Bioisosterism : a useful strategy for molecular modification and drug design, Curr. Med. Chem. 12 (2005) 23–49.

[39] R. Mikstacka, A.M. Rimando, K. Szalaty, K. Stasik, W. Baer-Dubowska, Effect of natural analogues of trans-resveratrol on cytochromes P4501A2 and 2E1 catalytic activities, Xenobiotica. 36 (2006) 269–285.

[40] R. Mikstacka, W. Baer-Dubowska, M. Wieczorek, S. Sobiak, Thiomethylstilbenes as inhibitors of CYP1A1, CYP1A2 and CYP1B1 activities, Mol. Nutr. Food Res. 52 (2008) 77–83.

[41] R. Mikstacka, A.M. Rimando, Z. Dutkiewicz, T. Stefański, S. Sobiak, Design, synthesis and evaluation of the inhibitory selectivity of novel trans-resveratrol analogues on human recombinant CYP1A1, CYP1B1 and CYP1B1, Bioorg. Med. Chem. 20 (2012) 5117–5126.

[42] M. Wierzchowski, Z. Dutkiewicz, A. Gielara-Korzańska, A. Korzański, A. Teubert, A. Teżyk, T. Stefański, W. Baer-Dubowska, R. Mikstacka,. Synthesis, biological evaluation and docking studies of trans-stilbene methylthio derivatives as cytochromes P450 family 1 inhibitors. *Chem. Biol. Drug. Des.* [Online early access]. DOI: 10.1111/cbdd.13042.

Published online: July 18, 2017.

[43] H. Yang, J.A. Baur, A. Chen, C. Miller, J.K. Adams, A. Kisielewski, K.T. Howitz, R.E. Zipkin, D.A. Sinclair, Design and synthesis of compounds that extend yeast replicative lifespan, Aging Cell 6 (2007) 35–43.

[44] L. Wang, K.W. Woods, Q. Li, K.J. Barr, R.W. Mccroskey, S.M. Hannick, L. Gherke, R.B. Credo, Y. Hui, K. Marsh, R. Warner, J.Y. Lee, N. Zielinski-mozng, D. Frost, S.H. Rosenberg, H.L. Sham, Potent, orally active heterocycle-based combretastatin A-4 analogues : synthesis, structure-activity relationship, pharmacokinetics, and in vivo antitumor activity evaluation, J. Med. Chem. 45 (2002) 1697–1711.

[45] C.M. Sun, L.G. Lin, H.J. Yu, C.Y. Cheng, Y.C. Tsai, C.W. Chu, Y.H. Din, Y.P. Chau, M.J. Don, Synthesis and cytotoxic activities of 4,5-diarylisoxazoles. Bioorg. Med. Chem. Lett. 17 (2007) 1078–1081.

[46] R. Romagnoli, P.G. Baraldi, O. Cruz-Lopez, C. Lopez Cara, M.D. Carrion, A. Brancale, E. Hamel, L. Chen, R. Bortolozzi, G. Basso, G. Viola, Synthesis and antitumor activity of 1,5-disubstituted 1,2,4-triazoles as cis-restricted combretastatin analogues, J. Med. Chem. 53 (2010) 4248–4258.

[47] R. Romagnoli, P.G. Baraldi, A. Brancale, A. Ricci, E. Hamel, R. Bortolozzi, G. Basso, G. Viola, Convergent synthesis and biological evaluation of 2-amino-4-(3’,4’,5’-trimethoxyphenyl)-5-aryl thiazoles as microtubule targeting agents, J. Med. Chem. 54 (2011) 5144–5153.

[48] R. Romagnoli, P.G. Baraldi, M.K. Salvador, D. Preti, M. Aghazadeh Tabrizi, A. Brancale,

X.H. Fu, J. Li, S.Z. Zhang, E. Hamel, R. Bortolozzi, G. Basso, G. Viola, Synthesis and evaluation of 1,5-disubstituted tetrazoles as rigid analogues of combretastatin A-4 with potent antiproliferative and antitumor activity, J. Med. Chem. 55 (2012) 475–488.

[49] R. Romagnoli, P.G. Baraldi, M.K. Salvador, M.E. Camacho, D. Preti, M.A. Tabrizi, M. Bassetto, A. Brancale, E. Hamel, R. Bortolozzi, G. Basso, G. Viola, Synthesis and biological evaluation of 2-substituted-4-(3′,4′,5′-trimethoxyphenyl)-5-aryl thiazoles as anticancer agents, Bioorganic Med. Chem. 20 (2012) 7083–7094.

[50] Ø.W. Akselsen, K. Odlo, J.J. Cheng, G. Maccari, M. Botta, V.T. Hansen, Synthesis, biological evaluation and molecular modeling of 1,2,3-triazole analogs of combretastatin A-1, Bioorg. Med. Chem. 20 (2012) 234–242.

[51] N.R. Madadi, N.R. Penthala, K. Howk, A. Ketkar, R.L. Eoff, M.J. Borrelli, P.A. Crooks, Synthesis and biological evaluation of novel 4,5-disubstituted 2H-1,2,3-triazoles as cis -constrained analogues of combretastatin A-4, Eur. J. Med. Chem. 103 (2015) 123–132.

[52] T.F. Greene, S. Wang, L.M. Greene, S.M. Nathwani, J.K. Pollock, A.M. Malebari, T. McCabe, B. Twamley, N.M. O'Boyle, D.M. Zisterer, M.J. Meegan, Synthesis and biochemical evaluation of 3-phenoxy-1,4-diarylazetidin-2-ones as tubulin-targeting antitumor agents, J. Med. Chem. 59 (2016) 90–113.

[53] V. Chaudhary, J.B. Venghateri, H.P.S. Dhaked, A.S. Bhoyar, S.K. Guchhait, D. Panda, Novel combretastatin-2-aminoimidazole analogues as potent tubulin assembly inhibitors: exploration of unique pharmacophoric impact of bridging skeleton and aryl moiety, J. Med. Chem. 59 (2016) 3439-3451.

[54] Z. Wang, H. Qi, Q. Shen, G. Lu, M. Li, K. Bao, Y. Wu, W. Zhang, 5-Diaryl-3H-1,2-dithiole-3-thiones and related compounds as combretastatin A-4/oltipraz hybrids: Synthesis, molecular modelling and evaluation as antiproliferative agents and inhibitors of tubulin, Eur. J. Med. Chem. 122 (2016) 520–529.

[55] A. Fürstner, F. Stelzer, A. Rumbo, H. Krause, Total synthesis of the turrianes and evaluation of their DNA-cleaving properties, Chem. Eur. J. 8 (2002) 1856–1871.

[56] P.S. Manchand, P.S. Belica, H. Wong, Synthesis of 3,4,5-trimethoxybenzaldehyde, Synth. Commun. 20 (1990) 2659–2666.

[57] F.M. Bevan, M.R. Euerby, S.J. Qureshi, The regioselectivity of lithiations in the synthesis of methoxymethylthiobenzaldehydes., J. Chem Res. Miniprint. 5 (1989) 901–920.

[58] S.C. Wong, S. Sasso, H. Jones, J.J. Kaminski, Stereochemical considerations and the antiinflammatory activity of 6-amino-6,7,8,9-tetrahydro-5H-benzocyclohepten-5-ols and related derivatives, J. Med. Chem. 20 (1984) 20–27.

[59] I. Kompis, A.E. Wick, Sulfur-containing substituted aldehydes, GB2087378A, 1982.

[60] D.A. Ramirez, J. Zhang, K. Klausmeyer, R.R. Kane, Synthesis and crystal structures of cis- and trans-1-(3′-N,N-dimethylthiocarbamoyl-4′-methoxy)-2-(3″,4″,5″trimethoxyphenyl) ethene, J. Chem. Crystallogr. 35 (2005) 227–232.

[61] L.K.A. Rahman, R.M. Scrowstone, 7-Substituted benzo[b]thiophenes and 1,2-benzisothiazoles. Part I . hydroxy- or methoxy-derivatives, J. Chem. Soc. Perkin Trans. I (1983) 2973–2977.

[62] Stefański, T.; Różański J.; Mikstacka, R.; Sobiak, S. The New Derivatives of (Z)-1,2-

Diphenylethene. WO2013/147629 A1, 2013.

[63] Stefański, T.; Różański, J.; Mikstacka, R.; Sobiak, S. The New Derivatives of (Z)-1,2-Diphenylethene. US2015/65727 A1, 2015.

[64] B. Biersack, K. Effenberger, S. Knauer, M. Ocker, R. Schobert, Ru(η6-arene) complexes of combretastatin-analogous oxazoles with enhanced anti-tumoral impact, Eur. J. Med. Chem. 45 (2010) 4890–4896.

[65] CombiGlide, version 3.3, Schrödinger, LLC, New York, NY, 2014.

[66] M.M. Mysinger, M. Carchia, J.J. Irwin, B.K. Shoichet, Directory of useful decoys, enhanced (DUD-E): better ligands and decoys for better benchmarking, J. Med. Chem. 55 (2012) 6582-6594.

[67] Y.K. Chiang, C.C. Kuo, Y.S. Wu, C.T. Chen, M.S. Coumar, J.S. Wu, H.P. Hsieh, C.Y. Chang, H.Y. Jseng, M.H. Wu, J.S. Leou, J.S. Song, J.Y. Chang, P.C. Lyu, Y.S. Chao, S.Y. Wu, Generation of ligand-based pharmacophore model and virtual screening for identification of novel tubulin inhibitors with potent anticancer activity, J. Med. Chem. 52 (2009) 4221–4233.

[68] C. Da, S.L. Mooberry, J.T. Gupton, G.E. Kellogg, How to deal with low-resolution target structures: using SAR, ensemble docking, hydropathic Analysis, and 3D-QSAR to definitively map the *αβ*-tubulin colchicine site, J. Med. Chem. 56 (2013) 7382-7395.

[69] R.B. Ravelli, B. Gigant, P.A. Curmi, I. Jourdain, S. Lachkar, A. Sobel, M. Knossow, Insight into tubulin regulation from a complex with colchicine and a stathmin-like domain, Nature 428 (2004) 198–202.

[70] LigPrep, version 3.0, Schrödinger, LLC, New York, NY, 2014.

[71] Epik, version 2.8, Schrödinger, LLC, New York, NY, 2014.

[72] Glide, version 6.3, Schrödinger, LLC, New York, NY, 2014.

[73] S. Mordalski, T. Kosciolek, K. Kristiansen, I. Sylte, A.J. Bojarski, Protein binding site analysis by means of structural interaction fingerprint patterns, Bioorg. Med. Chem. Lett. 21 (2011) 6816–6819.

[74] D.L. Hall, S.A.H. McMullen, Mathematical Techniques in Multisensor Data Fusion. 2nd ed.; Artech House, Inc, Norwood, MA, 2004.

[75] Instant JChem, version 5.3.1; ChemAxon (http://www.chemaxon.com).

[76] Canvas, version 2.0, Schrödinger, LLC, New York, NY, 2014.

[77] H. Wang, F. Wang, X. Tao, H. Cheng, Ammonia-containing dimethyl sulfoxide: an improved solvent for the dissolution of formazan crystals in the 3-(4,5-dimethylthiazol-2-yl)-2,5-diphenyl tetrazolium bromide (MTT) assay, Anal. Biochem. 421 (2012) 324–326.

[78] Q.Q. Li, R.X. Lee, H. Liang, Y. Zhong, E. Reed, Enhancement of cisplatin-induced apoptosis by *β*-Elemene in resistant human ovarian cancer cells, Med. Oncol. 30 (2013) 424.

Highlights

- A series of novel combretastatin A-4 (CA-4) thio analogues containing different molecular cores as tubulin polymerization inhibitors were synthesized.
- Parallel virtual screening protocol including the generation of a virtual combinatorial library was applied for design CA-4 analogues.
- The biological evaluation of target compounds comprised their cytotoxic, antitubulin and proapoptotic activities.
- Two lead compounds as oxazole-bridged analogues were identified.